MINISTRY OF EDUCATION AND SCIENCE OF UKRAINE

National Aerospace University Named by M. E. Zhukovsky
«Kharkov Aviation Institute»

Airplanedesign Faculty

Airplane and Helicopter Design Department

Explanatory Note
to Diploma Project of

Master

(degree)

Subject: Analysis of airborne liquid hydrogen cylinder ultimate load capacity

XAI.103.161F.23S.134. EN

Student of 6 Year 161 F Group
Speciality:134 Aerospace Engineering
Educational program:Aircraft and Helicopter design
Qiao Ruisheng
(name)
Supervisor: ass. prof, PhD, Chumak
(name)

Reviewer:

(name)

Kharkiv — 2023

Ministry of Education and Science of Ukraine
National Aerospace University named by M. E. Zhukovsky
«Kharkov Aviation Institute»

Department *Aircraft design*
Department *103 Aircraft and Helicopter Design*
Degree *Master*
Field of knowledge *13 Mechanical Engineering*
Speciality *134 Aerospace Engineering*
(Code and Name)
Educational program *Aircraft and Helicopter design*

APPROVED by
Head of Chair
PhD, Ass. Prof.
"____" _____2023___

T A S K
FOR QUALIFICATION PAPER

Qiao Ruisheng
(Name)

Subject of qualification paper Analysis of airborne liquid hydrogen cylinder ultimate load capacity

Supervisor of qualification paper Chumak Anton Sergeevich.
(name, degree, scientific degree)

Approved by University order No -уч from "0" 2023
Qualification paper presentation deadline 10.05.23
Initial data for the qualification paper Number of Passengers - 200
Range – 7200 km
L take-off -1.8 km
H cruising – 11 km
V crusing – 850 km/h

Content of explanatory note (list of problems to solve)

Summary

1. Designing section

1.1. Automated formation of the aircraft shape

Introduction, aim and tasks of design

1.1.1. Development of the aircraft concept, scientific and technical program to achieve its performance.

1.1.2. Gathering and processing of statistical Data, their analysis.
1.1.3. Selection and justification of the aircraft layout.
1.1.4. Calculation of aircraft zero approximation take-off mass.
1.1.5. Calculation of the weight of the design of main units of the plane, the mass of power fuel installation, equipment and control.
1.1.6. Determination of the power engine.
1.1.7. Determination of geometrical parameters for airplane units.
1.1.8. Determining the position of the center of mass.
1.1.9. Conclusions.

1.2. Analysis of optimized aircraft design parameters influence on its aerodynamic and mass characteristics..

1.2.1. Calculation of Lift Coefficient, Drag Coefficient and Lift-to-Drag Ratio during Takeoff.
1.2.2. Calculation of Performance of Takeoff.
1.2.3. Calculation of Performance of Landing.
1.2.4. Conclusion.

2. Economics

Calculation of aircraft cost and transportation cost.

3. Special task

Analysis of airborne liquid hydrogen cylinder ultimate load capacity

3.1. Development of sustainable aircraft.

3.1.1 Solar aircraft.
3.1.2 Energy storage battery aircraft.
3.1.3 Hydrogen-powered aircraft.
3.1.4 Biofuel aircraft.

3.2. Review of hydrogen storage.

3.3. Theoretical Background of liquid hydrogen storage.

3.4. Analysis of airborne liquid hydrogen cylinder ultimate load capacity.

3.5. Modelling and simulation.

3.6. Theoretical Buckling Analysis of outer container.

List of drawings

- Master geometry of aircraft surface, general view drawing ;
- Master geometry of the unit;
- Analytical models of designed unit parts, subassemblies;
- Theoretical drawing of the unit;
- Assembly drawing of the unit.

Advisors of qualification paper sections

Section		Name and duty of advisor	Signature, Date	
			Task is given	Task is passed
1.	**Designing section**	**Chumak A.S.**		
2.	**Economical section**	**Pavlenko T.Y.**		
3.	**Special section**	**Chumak A.S.**		

Normative inspection_____ ____ «____» _____2023__
(Sign) (Name)

Date when task is given_____

3. CALENDAR PLAN

Nos	Qualification paper milestones	Paper milestone deadlines	4. Notes
1.	**Designing section**	**4.12**	
2.	**Economical section**	**4.20**	
3.	**Special section**	**5.08**	

Applicant _____ **Qiao Ruisheng**
(Sign) (Name)

Supervisor of paper _____ Chumak Anton Sergeevich.
(Sihn) (Name)

ABSTRACT

Master degree thesis "Analysis of airborne liquid hydrogen cylinder ultimate load capacity"

The thesis contains 70 pages, 31 figures, 11 tables and 30 references.

The purpose of this work is to do the preliminary design of the aircraft, review and prospect of the sustainable aircraft and analyse the liquid hydrogen cylinder ultimate load capacity in hydrogen aircraft.

The main object of this paper is the liquid hydrogen cylinder, which is a double-layer structure. The inner cylinder is mainly made of A5083 aluminum alloy with excellent low temperature performance while the outer cylinder is made of S30408 stainless steel. And the high vacuum multi-layer insulation is used between them. Since the ultimate load carrying capacity of the liquid hydrogen cylinder is relatively dangerous and costly, this research uses numerical simulation to investigate the ultimate load carrying capacity of the cryogenic liquid hydrogen cylinder.

In the research, the three-dimensional numerical model of the cylinder was established and the finite element calculation method was used to calculate the ultimate load carrying capacity of airborne liquid hydrogen cylinder. The research results are as follows.

(1) A numerical simulation model of the cylinder container was established, and the ultimate load carrying capacity of the inner cylinder was analyzed using the ultimate load method and the elastic-plastic analysis method. The simulation results show that the structure meets the requirements.

(2) The stability analysis of the outer cylinder is carried out, and the wave number and critical instability load when instability occurs in the shell are calculated theoretically.

Key words: sustainable aircraft, hydrogen aircraft, airborne liquid hydrogen cylinder, ultimate load capacity analysis

CONTENT

1 DESIGN SECTION

1.1 Statistical Designing of the Aircraft Shape

1.1.1 Development of technical task

From the 1970s to the present, global carbon emissions have basically shown a positive correlation with global economic development. In terms of total emissions and growth rate, global carbon emissions show a synchronous upward trend with total economic volume, but the growth rate has slowed down in recent years, especially during the global epidemic.

With the development of technology, the thrust of aircraft engines has increased significantly. And the safety has also improved greatly. The twin-engine design is sufficient to support long-range flights. Both fuel economy and maintenance costs are much lower compared with four engines. In recent decades, Environmental protection and green aviation are major directions in the development of today's air transport industry, and how to reduce carbon emissions has long been a major concern for the aviation industry.

New energy vehicles have gained an extremely wide range of applications. On September 22, 2020, Chinese President Xi Jinping proposed that China strive to reach peak CO2 emissions by 2030 and work towards achieving carbon neutrality by 2060. The European Aviation Safety Agency and industry are also making active efforts on reducing carbon emissions from currently operating aircraft. On the one hand, they have issued policies to minimize fuel consumption of flights, and on the other hand, they are developing and promoting sustainable aviation fuels.

Design an aircraft with the great performance is a complicated and integrated problem. It requires a set of optimization tasks in many aspects, including geometrical, aerodynamic, structural, flight-technical and economic characteristics, etc. It is a self-contradictory problem requires other sacrificial design aspects. For this reason, a good design is a comprehensive balance for the purpose.

During the process of design, in the first place we need to be clear the usage of the aircraft, find some prototypes and use statistical information, empirical references and some other methods to do a full aerodynamic calculation and analysis. Besides, doing some experiments or wind tunnel experiments are beneficial to get the first-hand data.

Considering the prototype is a large aircraft, it needs to meet the Certification Specifications for Large Airplanes CS-25 or FAR-25. For utility aircraft, it meets CS-23 or FAR 23. However, the current U.S. FAR 23 does not contain provisions dedicated to the certification of new energy aircraft. EASA released an airworthiness validation framework document for new vertical takeoff and landing (VTOL) versions in 2019, which provides guidance on the airworthiness framework for new all-electric and hybrid models, covering a wide range of VTOL types including multi-rotor and tilt-rotor, such as sc-VTOL-01. The official policy documents for eVTOL airworthiness validation is used in collaboration with CS-25. The Civil Aviation Administration of China (CAAC) uses D0311, ASTM2840 and other standards for electric propulsion systems to complete the airworthiness validation of electric aircraft. In 2020, it prepared the final draft of Chapter H Airworthiness Validation Guide and Technical Specification of Electric Propulsion System for Electric Aircraft about the new version of Part 23, which promoted the development of electric aircraft validation system [1].

A new aircraft is going to be designed by taking into account the similar series of airplanes. The basic tactical and technical requirements are shown in table 1.1.

Table 1.1 – Tactical and Technical requirement

N, passenger	Range, km	$V_{cruising}$, km/h	$H_{cruising}$, km	$L_{take\text{-}off}$, km
200	7200	850	11.9	1.8

1.1.2 Gathering and processing of statistical Data, their analysis

By referring the basic tactical and technical requirements, here five prototypes are listed in the preliminary design, Airbus 321neo, 320neo, A321, A320 and Boeing 737max9. The statistical data are shown in Table 1.2. The table provides the possibility to select the great characteristics for the new aircraft.

Table 1.2 – Statistical parameters of Prototypes

	PLANES				
	A321neo	A320neo	A321	A320	B737max9
Crew/flight attendant	2/6	2/5	2/6	2/5	2/5
Max takeoff weight, m_{tow}, kg	97000	79000	93500	78000	88314
Passenger's seat	240	195	220	180	193
The height of the flight $H_{f.}$, m	12100	12100	12100	12100	12000
Most pay-load, $m_{c.max}$, kg	25500	20000	25300	19900	20882
Range $m_{к.max}$, km	7400	6500	5930	6612	6570
Take off distance L, m	1988	1951	2210	2100	2600
Landing distance, m	1600	1600	1600	1500	1700
Cruising speed, V, km/h	828	828	828	828	839
Cruising height, H_{cru}, m	11900	11900	11900	11900	11800
Number and type of engines	2×CFM International LEAP-1A	2× Pratt & Whitney PW1100G	2×CFM 56-5B	2×CFM 56-5B	2×CFM International LEAP-1B
Thrust of each engine, KN	160	160	140	140	130

End of table 1.2

Pressure ratio	50	50	35	35	40
Bypass ratio	12.5	12.5	6	6	9
Length of aircraft, m	44.51	37.57	44.51	37.57	42.16
Height of aircraft, m	11.76	11.76	11.76	11.76	12.3
Diameter of fuselage, m	3.95	3.95	3.95	3.95	3.76
Wingspan, L_w, m	35.80	35.80	35.80	35.80	35.92
Wing aspect ratio, λ_w	9.390	9.390	9.395	9.350	9.442
Wing taper ratio, η_w	0.240	0.240	0.240	0.240	0.278
Wing sweepback on 1/4 chord, $\chi_{1/4}$, °	25	25	25	25	25

1.1.3 Selection and justification of the aircraft layout

The aircraft layout and shape directly influence the aerodynamic properties and the position of the center of gravity. And wing design determines the range, speed, operational envelope, etc. The configuration of this aircraft is conventional since it is designed for long-range passenger aircraft. Sweptback, low wing design can relatively reduce the cost of fuel, increase speed and safety especially when it is ditching in an emergency.

1.1.4 Calculation of aircraft zero approximation take-off mass

Aircraft take-off mass is one of the most important parameters in aircraft design. The calculation of aircraft zero approximation take-off mass is made when the designer has chosen the aircraft configuration. lt is calculated by the following formula:

$$m_o = \frac{m_{crew}+m_{payload}}{1-(\bar{m}_{airframe}+\bar{m}_{pp}+\bar{m}_{cs}+\bar{m}_f)}$$

Where, m_{crew} - the mass of service load and crew. It is assumed that the average weight of each crew member is 80 kg;

$$m_{crew} = m_{crew} \times n_{crew} = 80 \times 7 = 560 \text{ kg}.$$

$m_{payload}$ - the mass of payload;

Mass of payload for passenger airplanes is assumed that the mass of one passenger including luggage is 110 kg. The number of passengers n is equal to 110.

$$m_{payload} = n \times n_{PAS} = 110 \times 200 = 22000 \text{ kg}.$$

$\bar{m}_{airframe}$ – Relative mass of the frame, which consists of the relative mass of the wing, fuselage, tail unit and landing gears;

$\bar{m}_{pp}$ – Relative mass of the power plant, which includes the relative mass of the engine plus mounting and servicing system;

$\bar{m}_{cs}$ – Relative mass of the control system and equipment, including the mass of the hydraulic system, pneumatic system, navigation equipment and surface control devices;

$\bar{m}_f$ – the relative mass of fuel, which is calculated by empirical formula.

$$\bar{m}_f = a + b\frac{L}{V_{CR}} = 0.06 + 0.05 \times 7200/850 = 0.46.$$

Where, L - the flight range, L = 7200km;

V_{cr} - the cruise flight speed, V_{cr} = 850km/h;

Coefficient $a = 0.06$, $b = 0.05$.

Table 1.3 - Ranges of Relative Masses of Airplane Units and Fuel

Plane purpose		$\bar{m}_{airframe}$	$\bar{m}_{pp}$	$\bar{m}_{cs}$	$\bar{m}_f$
Subsonic passenger long-range	Light	0.30~0.32	0.12~0.14	0.12~0.14	0.18~0.22
	Medium	0.28~0.30	0.10~0.12	0.10~0.12	0.26~0.30
	Heavy	0.25~0.27	0.08~0.10	0.09~0.11	0.35~0.40
Supersonic passenger		0.20~0.24	0.08~0.10	0.07~0.09	0.45~0.52

Compared with the reference in table 1.3, the result is far beyond the standard. So we decide to use more precise method to calculate the relative mass of fuel.

More precisely the value of passenger aircraft is calculated using this relation:

$$\bar{m}_f = 1.1\left(1 - e^{-\frac{L*C_{cons}}{V_{cr}*K_{max}}}\right)$$

Where, C_{cons} - the specific fuel consumption, kg/daN-h;

K_{max} - the maximum lift-to-drag ratio.

Here we assume $C_{cons} = 0.45$, $K_{max} = 13.6$, then get $\bar{m}_f = 0.29$

Considering the type of aircraft is long-range, this result is reasonable.

According to the reference, for long-range, medium passenger aircraft,

$\bar{m}_{airframe} = 0.28;\ \bar{m}_{pp} = 0.10;\ \bar{m}_{cs} = 0.19.$

At last we can get the take-off mass of the aircraft in the zero approximation $m_0 = 98t$.

1.1.5 Calculation of the weight of the design of main units of the plane, the mass of power fuel installation, equipment and control

After determining the take-off weight of the aircraft, we can calculate the weight of the design of main units of the airplane according to the guide book. Different aircraft types correspond to different calculation ranges. The results are shown in table 1.4.

Table 1.4 – The weight of the design of main units of the plane

$\mathbf{m}_0$, kg	$\mathbf{m}_f$, kg	$\mathbf{m}_{pp}$, kg	$\mathbf{m}_{cs}$, kg	$\mathbf{m}_{frame}$, kg			
				$\mathbf{m}_{wing}$, kg	$\mathbf{m}_{fuselage,}$ kg	$\mathbf{m}_{tail\ unit}$, kg	$\mathbf{m}_{landing\ gear}$, kg
1	0.29	0.10	0.10	0.109	0.10	0.02	0.051
98000	28420	9800	9800	10646	9823	2003	4967
				27440			

1.1.6 Determination of the power engine

From the guide, we know that the relative mass of engine is:

$$\overline{m}_{\text{p.p}} = R\gamma_{en}t_0$$

Where, R - coefficient considering power plant mass increment in comparison with engines' mass;

$$\text{R} = k_1(1+0.1\frac{n_{en.rev}}{n_{en}})(1+\frac{0.0236}{\gamma_{en}}(1.5+0.275y^{0.75})^2)$$

K_1 - coefficient considering number and arrangement of engines in airplane;

n_{en} - number of engines in airplane;

$n_{en.rev}$ - number of engines with reverser;

γ_{en} - specific weight of engines;

y - bypass ratio of engines.

Specific weight for the engine can be estimated:

$$\gamma_{en} = 0.22 - 0.0288y + 0.0077y^{1.5}$$

Thrust-weight ratio for calculations is determined on the basis of the following requirements: providing cruising flight with given speed at given altitude, given takeoff run and providing continuous takeoff with one engine inoperative.

Thrust-weight ratio for providing cruising flight is calculated:

$$t_{0crus} = \frac{0.7 P_H M_{crus}^2 C_{xcrus}}{\xi_V \xi_H \xi_{thr} \xi_{t-off} p}$$

During cruising flight stage:

$$C_{xcrus} = \frac{4}{3} C_{x0} = \frac{4}{3}(\mathrm{F}_1 + F_2 p)$$

$F_1 = K_{t\text{-}unit} C_{xwing}$

$K_{t\text{-}unit}$ - tail unit loading;

C_{xwing} - wing drag coefficient;

$F_2 = C_{xfus}/K_{mids}$ umber of engines in airplane;

K_{mids} - midsection loading, daN/m^2;

C_{xfus} - fuselage drag coefficient;

p - atmospheric pressure at cruising altitude;

ξ_V, ξ_H, ξ_{thr} - coefficients accounting variation of engine thrust in proportion to speed,altitude and engine operation regime,are taken from ratings of similar engines for M_{crus};

$\xi_{t\text{-}off}$ - takeoff coefficient at H=0 and $M_{t\text{-}off}$.

$$\xi_{t-off} = \xi_V \xi_H \xi_{thr} \xi_{airintake}$$

Thrust-weight ratio required for specified takeoff run is calculated by:

$$t_{0p} = \frac{1}{\xi_{t-off}} \left(\frac{0.832 p}{L_p C_{yt-off}} + \frac{1}{3} \left(\frac{1}{K_{t-off}} + 2f \right) \right)$$

$\xi_{airintake}$ - coefficient considering thrust losses related with loss of dynamic head in air intake;

L_p - takeoff run, m;

f - wheel friction coefficient over runway surface while takeoff running. f=0.02-0.03 for dry concrete.

Thrust-weight ratio required to provide continuous takeoff with one engine inoperative during takeoff run,

$$t_{0\theta} = \frac{n_{en}}{\xi_{t-off}(n_{en}-1)}\left(\frac{1}{K_{t-off}} + tg\theta_3\right)$$

$tg\theta_3$ - climb gradient during the third takeoff stage with one engine inoperative, which specified in Airworthiness Requirements.

After the calculation, the result shows that the aircraft Thrust-Weight ratio $t_0 = 0.32$ would be adequate to meet the takeoff requirement. The performance of Thrust-weight ratio t_0 and wing aspect ratio λ in proportion to wing loading p at different stage is shown in figure 1.1.

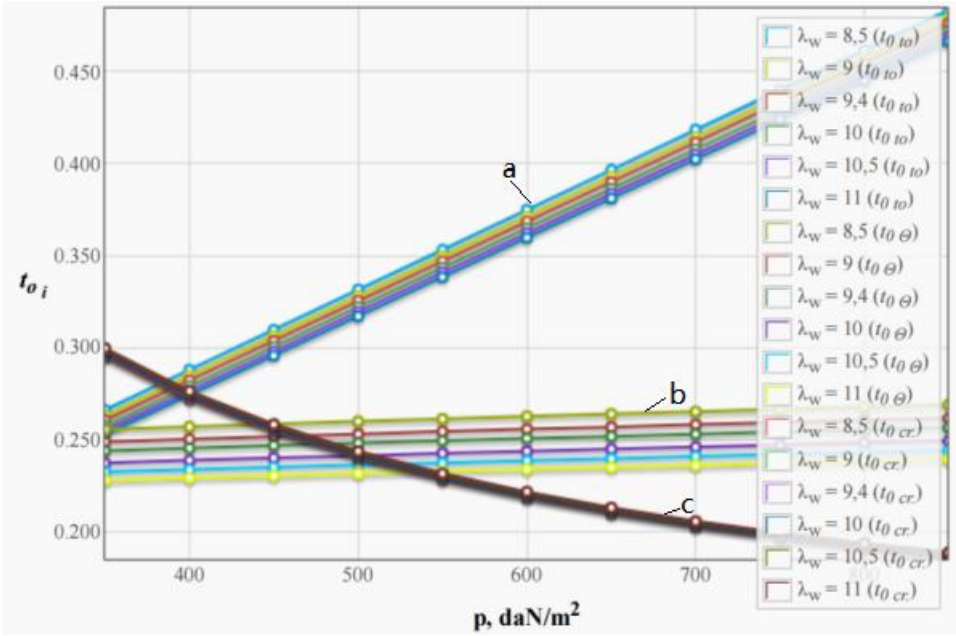

Figure 1.1 - Thrust-weight ratio t_0 and wing aspect ratio λ in proportion to wing loading p at different stage

a- Thrust-Weight ratio required to provide given takeoff run;

b- Thrust-Weight ratio required to provide continuous takeoff with one engine inoperative during takeoff run;

c- Thrust-Weight ratio required to provide cruising flight with $M_{crusing}$ at $H_{crusing}$.

From the figure 1.1, we know that the Thrust-Weight ratio required to provide continuous takeoff with one engine inoperative during takeoff run is 0.23 and Thrust-Weight ratio required to provide cruising flight is 0.25.

The total thrust of the aircraft is equal to:

$$P_0 = t_0 * m_0 * g = 0.32 * 98000 * 9.8 = 307\ kN$$

The thrust of one engine is equal to:

$$P_1 = \frac{P_0}{n} = \frac{307}{2} = 153.5kN$$

Considering the power and environmental requirements, we choose CFM International LEAP 1A from the available engine, which is a twin spool, high bypass turbofan engine. The thrust reaches 160 KN. It is widely used on A320 family and B737max. Its parameters and picture are shown in table 1.5 and figure 1.2.

Table 1.5 - Parameters of CFM International LEAP 1A

Model	Thrust (KN)	Bypass ratio	Pressure ratio	Wet weight (Kg)
CFM International LEAP 1A	160	11	40	990

Figure 1.2 - CFM International LEAP 1A

1.1.7 Determination of geometrical parameters for airplane units

1.1.7.1 Determination of the geometric parameters of the wing:

The wing loading is crucial because it is directly related to the

aircraft aerodynamic and aeromechanical performance in fixed wing configuration [2]. And we continue further calculation of geometric parameters of the wing.

According to the former calculation result, we know that the specific load P_0 on the wing during takeoff is equal to 500 daN/m^2, which equals to 5000 N/m^2.

Wing aera $S_{wing} = \frac{m_0 \cdot g}{P_0} = \frac{98000*9.8}{5000} = 192m^2$;

Wing span $1 = \sqrt{(S_w \cdot \lambda_w)} = \sqrt{(192*9.4)} = 42.52m$;

Root chord is: $b_0 = \frac{2 \cdot S_w \cdot \eta_w}{(1+\eta_w) \cdot 1} = \frac{2*192*4.11}{5.11*42.52} = 7.264m$;

Tip chord is: $b_t = \frac{b_0}{\eta_w} = \frac{7.264}{4.11} = 1.78m$;

Mean aerodynamic chord (MAC) in meters is calculated by the formula:

$$b_{MAC} = \frac{2 \cdot b_t}{3} \cdot \frac{1+\eta_W+\eta^2{}_w}{(1+\eta_W)\eta_W} = \frac{2*7.264*(1+4.11+4.11*4.11)}{3*5.11*4.11} = 5.07\text{m}$$

The aileron is a small movable airfoil mounted on the outside of the trailing edge of the wing tip. And it is the primary operating rudder surface of the aircraft. The pilot manipulates the roll moment generated by the differential deflection of the left and right ailerons to make the aircraft do a roll maneuver.

Ailerons span: $l_{ail} = 0.378 \cdot \frac{l_w}{2} = 0.378* \frac{42.52}{2} = 8.03m$;

Aileron area: $S_{ail} = 0.066 \cdot \frac{S_w}{2} = 0.066* \frac{192}{2} = 6.34m^2$;

Aileron chord: $b_{ail} = (0.22 \sim 0.26) \times b_t = 0.24 \times 1.78 = 0.427$ m;

Aileron area: $S_{ail} = (0.05 \sim 0.08) \times S_w / 2 = 0.065 \times 192/2 = 6.24$ m^2.

Naturally, the wing needs to be equipped with a high lift device to increase lift, improve airflow and shorten takeoff and landing distances by increasing the curvature of the wing profile and the angle of attack. Here table 1.6 shows the ranges of the rate of relative chord for different types of high lift devices.

Table 1.6 - Ranges of the rate of Relative chord

High lift devices	The rate of its relative chord
split edge flaps	0.25 ~ 0.3
one slotted or two slotted flaps	0.28 ~ 0.3
Faylers flaps	0.3 ~ 0.4
slats	0. 1 ~ 0. 15

For prototype A321neo, it adapts the two-slotted flap design.

The flap chord is: $b_{fl} = (0.28 \sim 0.3)\, b_t = 0.29 \times 1.78 = 0.493$ m.

1.1.7.2 Determination of the geometric parameters of the fuselage:

Fuselage length is equal: $l_f = \lambda_f \cdot D = 11.26 * 3.95 = 44.48m$;

Length of the fuselage nose section: $l_{fnp} = \lambda_{fnp} \cdot D_f = 1.8 * 3.95 = 7.11m$;

Length of the fuselage aft section: $l_{frp} = \lambda_{frp} \cdot D_f = 2.64 * 3.95 = 10.43m$.

1.1.7.3 Determination of the geometric parameters of the tail unit:

Area of vertical tail unit: $S_{VTU} = \frac{l_w \cdot S_w}{L_{VTU}} \cdot A_{VTU} = \frac{42.52 * 192}{15.3} * 0.1 = 53.36 m^2$;

Area horizontal tail unit: $S_{HTU} = \frac{b_{MAC} \cdot S_w}{L_{HTU}} \cdot A_{HTU} = \frac{5.1 * 192}{15.3} * 0.73 = 46.72 m^2$;

Elevator area: $S_{el} = (0.3 \sim 0.4) \cdot S_{HTU} = 0.37 * 46.72 = 17.3 m^2$;

Rudder area: $S_{rud} = (0.35 \sim 0.45) \cdot S_{VTU} = 0.4 * 53.36 = 21.8 m^2$.

Span of Horizontal Tail Unit and Vertical Tail Unit for low wing aircraft:

$L_{HTU} = (0.32 \sim 0.5)\ l_w = 0.4 * 42.52 = 17m$;

$H_{VTU} = (0.14 \sim 0.2)\ l_w = 0.18 * 42.52 = 7.65m$.

Tip and Root chord of horizontal stabilizer is equal to:

$b_{tHTU} = \frac{2 \cdot S_{HTU}}{(1+\eta_{HTU}) l_{HTU}} = \frac{2 * 46.72}{(1+2.67) * 17} = 1.5$m;

$b_{rHTU} = b_{tHTU} \cdot \eta_{HTU} = 1.5 * 2.67 = 4m$;

Horizontal Stabilizer Mean Aerodynamic Chord is

$$b_{HAS} = \frac{2 \cdot b_{HTU}}{3} \cdot \frac{1 + \eta_{HTU} + \eta^2_{HTU}}{(1 + \eta_{HTU})\eta_{HTU}} = \frac{2 * 4 * (1 + 2.67 + 2.67 * 2.67)}{3 * 3.67 * 2.67} = 2.94\text{m}$$

Tip and Root chord of vertical stabilizer is equal to:

$$b_{tVTU} = \frac{2 \cdot S_{VTU}}{(1 + \eta_{VTU})h_{VTU}} = \frac{2 * 53.36}{(1 + 3.67) * 7.65} = 2.98\text{m};$$

$b_{rVTU} = b_{tVTU} \cdot \eta_{VTU} = 3 * 3.67 = 10.9m$;

Vertical Stabilizer Mean Aerodynamic Chord is

$$b_{VAS} = \frac{2 \cdot b_{VTU}}{3} \cdot \frac{1 + \eta_{VTU} + \eta^2_{VTU}}{(1 + \eta_{VTU})\eta_{VTU}} = \frac{2 * 10.9 * (1 + 3.67 + 3.67 * 3.67)}{3 * 4.67 * 3.67} = 7.72\text{m}$$

1.1.7.4 Determination of the geometric parameters of the landing gear:

In figure 1.3, the wheel track T is expressed by B and the landing gear wheel base B is expressed by b.

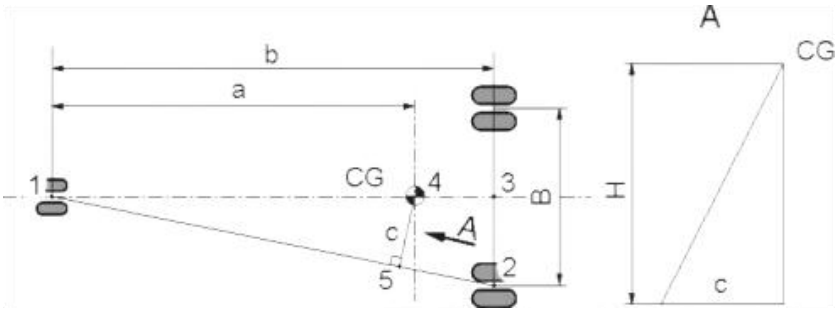

Figure 1.3 - Scheme of Definition of Minimal Wheel Track of Nose-Wheel Configuration

Main wheel axel offset is: $B_M = 0.25 \cdot b_{MAX} = 0.25 * 5.1 = 1.3\text{m}$;

Landing gear wheel base: $B = 0.4 \cdot l_f = 0.4 * 44.48 = 17.8m$;

Front wheel axial offset equals: $B_n = B - B_M = 17.8 - 1.3 = 16.5\text{m}$;

Wheel track is: $T = 0.6 \cdot B = 0.6 * 17.8 = 10.68m$.

In terms of ICAO Standards of aerodrome classification, if wingspan is within 36~52m, distance between Outer Main Wheels have to be in 9~14m. Therefore, 10.68m is within the range which meets the requirements.

According to the scheme and geometric knowledge, we get c = 4.74m and landing gear height H = 2.8 m.

The load on Nose wheel is equal to:

$$P_{nose} = \frac{9.81 \cdot B_M \cdot m_0 \cdot K_g}{B \cdot z_{nose}} = \frac{9.81 * 1.3 * 98000 * 1.75}{17.8 * 2} = 61436 \text{ N}$$

Where - the dynamics coefficient K_g = 1.5 ~ 2.0;

z - the number of wheels on each support;

n - the number of supports.

The load on main wheel is equal to:

$$P_{main\ wheel} = \frac{9.81 \cdot B_n \cdot m_0}{B \cdot z \cdot n} = \frac{9.81 * 16.5 * 98000}{17.8 * 2 * 4} = 111395 \text{ N}$$

1.1.8 Determining the position of the center of mass

To keep balance and stability during flight, takeoff and landing, considering the fuel weight change and other factors, the position of the aircraft center of mass must be maintained in a certain range. The aircraft has strict rules for the position of the center of gravity, with a front limit and a rear limit. In this part, we have not considered the variation of it. For the zero approximation of CG positions, we assume it:

X_m - The distance for the center of mass from nose part to mean aerodynamic, indicated in figure 1.4.

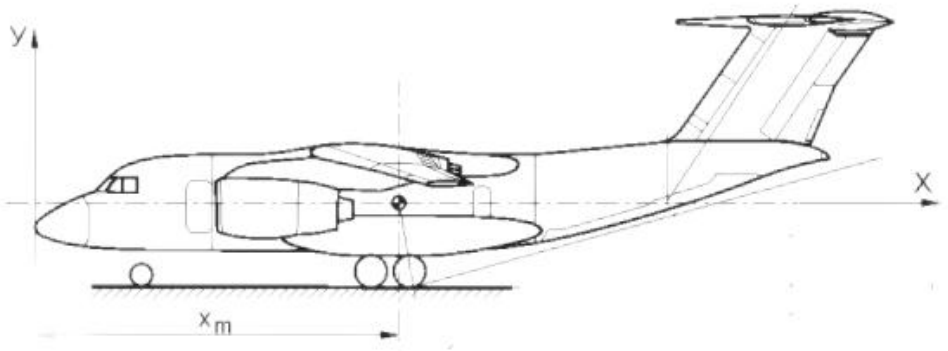

Figure 1.4 - Scheme of position of center of mass

For airplanes with swept wing (x = 30 ~ 40°), distance from the center of mass to the nose of the wing MAC.

$$X'_{W} = (0.26 \sim 0.30) \cdot b_A = 0.28 * 5.1 = 1.43\text{m}$$

Fuselage CG is positioned at 0.6L for swept-wing,

$$X_F = 0.6 \cdot L = 0.6 * 44.48 = 26.69\,\text{m}$$

The equation for calculation of X_m is:

$$m_f \cdot X_F + m_w \cdot (X_M + X'_w) = m_0 \cdot (X_M + C)$$

Where, C - the distance from leading edge MAC to the center of aircraft gravity point and for commercial airplane with low wing, C = (0.22~0.25)*b_{MAC}

At last, we get the result:

$$X_M = \frac{m_f X_f + m_w \cdot X'_w - m_0 C}{m_0 - m_w} = 22.04\text{m}$$

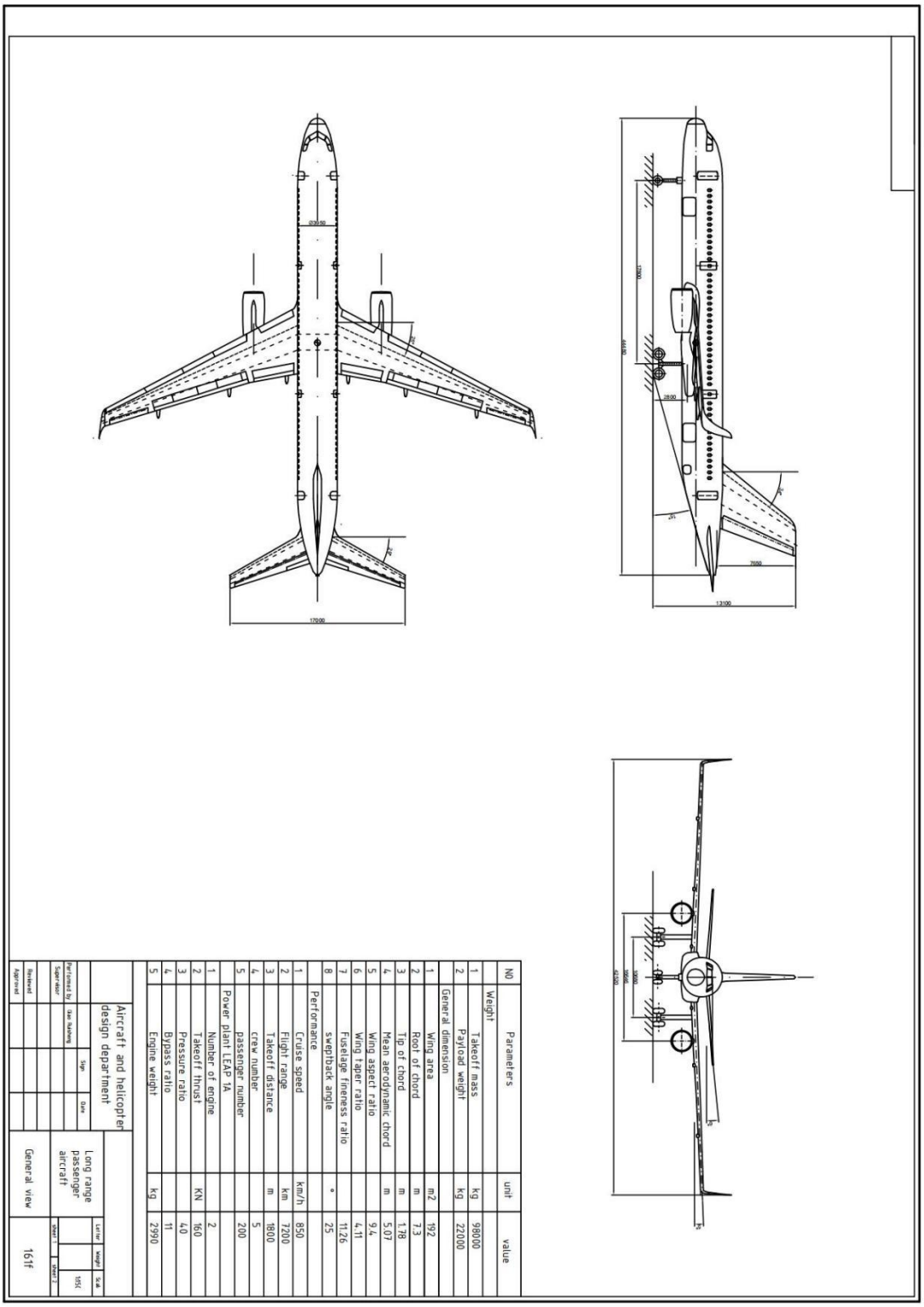

Figure 1.5 - The general view drawing of the aircraft

1.1.9 Conclusions

After zero approximation, we get the basic parameters and layout of the airplane. There are more precise results in further approximations. And by applying more advanced technology, the performance of the aircraft will be even better. The general view drawing of the aircraft is shown in figure 1.5.

The prevailing trend of aircraft is energy saving and green, high speed and efficient, safe and reliable. The aircraft design in this paper meets the international and Chinese primary requirements.

1.2 Aircraft Aerodynamic and Flight Performance Calculations

1.2.1 Calculation of Lift Coefficient, Drag Coefficient and Lift-to-Drag Ratio during Takeoff

After the first part, we get the basic parameters of the airplane. Here we consider its aerodynamic performance.

Formula for determining lift coefficient during takeoff is:

$$C_{yt-off} = C_{yw.t-off}(1 + \Delta\overline{C_y}\frac{\delta_{flapt-off}}{\delta_{flaptble}} \cdot \frac{b_{flap}}{\overline{b}_{flaptble}}\overline{S_{highlift}}\cos^2\chi_{0.75}) + \Delta C_{yground} + \Delta C_{y\text{blow}}$$

Here $C_{yw.t-off}$ - wing lift coefficient without high-lift devices:

$$C_{yw.t-off} = C_y^{\alpha} \cdot \alpha_{t-off}$$

α_{t-off} - wing angle-of-attack during takeoff at lift-off moment, degree;

C_y^{α} - derivative of wing lift coefficient on angle of attack, 1/deg.

$$C_y^{\alpha} = \frac{0.11 - 0.029\sqrt[4]{\overline{c}}}{1/\cos\chi_{1/4} + 2/\lambda}$$

$\Delta\overline{C_y}$ - increase of lift coefficient due to application of high-lift devices;

$\delta_{flapt-off}$ - takeoff flap angle, degree;

$\delta_{flaptble}$ - slat angle from table, degree;

$\bar{b}_{flap}$ - flap relative chord;

$\bar{b}_{flaptble}$ - flap relative chord from table;

$\overline{S_{highlift}}$ - wing relative area, occupied by high-lift devices in takeoff position;

$$\overline{S_{highlift}} = (\frac{2\eta - \overline{l_{flap}}(\eta - 1)}{\eta + 1} + k_{flap})\overline{l_{flap}} + k_{slat}\overline{l_{slat}}$$

$\eta = \mathrm{b}_0 / b_{wing}$ - wing taper;

b_0 - wing root chord;

b_{wing} - wing tip chord;

$\overline{l_{flap}}$ - flap relative span;

k_{flap} - flap lift-to-drag ratio;

$\overline{l_{slat}}$ - slat relative span;

k_{slat} - slat lift-to-drag ratio;

$\chi_{0.25}$, $\chi_{0.75}$ - wing sweep in degrees correspondingly at 0.25 and 0.75 of chord;

$\Delta C_{yground}$ - increase of ΔC_y due to ground effect table;

$\Delta C_{yground} = 0.313 - 0.237\bar{\mathrm{h}} + 0.0572(\bar{h})^2$

$\bar{\mathrm{h}} = \mathrm{h} / b_{mac}$ - wing position relative height;

h - distance from end of b_{mac} to the ground level;

b_{mac} - wing mean aerodynamic chord;

$\Delta C_{y\mathrm{blow}}$ - increase of ΔC_y due to wing blowing by propellers, for turbofan engine, $\Delta C_{y\mathrm{blow}} = 0$.

Airplane lift-to-drag ratio during takeoff is calculated by the following formula:

$$\mathrm{K}_{t-off} = \frac{C_{yt-off}}{C_{xt-off}}$$

$$C_{xt-off} = C_{x0t-off} + \Delta C_{x\mathrm{LG}} + C_{x\mathrm{flap}} + A_{ground} C^2{}_{yt-off}$$

$C_{x0t-off}$ - airplane drag coefficient at zero lift for Mach number corresponding lift-off speed M_{t-off} during takeoff;

$\Delta C_{x\mathrm{LG}}$ - increase of airplane drag coefficient due to extended LG;

$$\Delta C_{x\mathrm{LG}} = 0.012 + 0.1 C_{x0\mathrm{t}-off}$$

$C_{x\mathrm{flap}}$ - increment of airplane drag coefficient due to extended flaps;

$$C_{x\mathrm{flap}} = \overline{S}_{highliftt-off}(6\overline{\mathrm{b}}_{flap} - 0.22)(6.35*10^{-4}\delta_{flapt-off} + 2.44*10^{-5}\delta^2{}_{flapt-off})$$

A_{ground} - polar coefficient accounting ground effect;

$$A_{ground} = \frac{2.8k_2(1+\overline{S}_{fusenac})}{k_1\lambda(\bar{l}+7.4)}$$

$$C_{x0t-off} = 1.1(k_{t-unit}C_{xwingt-off} + \frac{p}{k_{mids}}C_{xfuset-off})$$

$$k_{\text{t-unit}} = 1 + \overline{S}_{HS} + \overline{S}_{VS}$$

$k_{\text{t-unit}}$ - coefficient accounting increment of airplane drag due to tail unit;

k_{mids} - midsection loading, daN/m^2 .

k_1 - coefficient accounting influence of wing sweep upon effective aspect ratio;

$$k_1 = 1 + 6.667*10^{-4}\chi_{0.25} - 7.728*10^{-5}\chi^2{}_{0.25}$$

k_2 - coefficient accounting influence of geometrical aspect ratio upon effective aspect ratio. k_2=1.02 for aspect ratio $\lambda > 6$.

$\bar{\mathrm{l}} = 1/h$ - wing relative span;

h - distance from end of b_{mac} to the ground level;

$\overline{S}_{fusenac}$ - wing relative area occupied by fuselage, engine nacelles, and Landing Gear sponsons.

For the airplane designed, the Wing high-lift devices type is Slat and double slotted retractable flap.

$\Delta\overline{C_y} = 2.0$, $\overline{l_{slat}} = 0.85$, $\overline{l_{flap}} = 0.7$, $\bar{b}_{flap} = 0.28$, $k_{flap} = 0.14$, $\delta_{flapt-off} = 30$, $\alpha_{t-off} = 15$, $\bar{h} = 0.63$, $M_{t-off} = 0.2$, $k_{mids} = 7000$, $\bar{l} = 13$

After calculation, we get the result of wing aspect ratio influence on take-off lift coefficient C_y and wing loading influence on lift-to-drag ratio K_{t-off} , which shown in figure 1.5 and figure 1.6 respectively.

From the results, we know that with the increase of wing aspect ratio, the lift coefficient and lift-to-drag ratio are increase as well since it reduces the induced drag. But the increase of wing aspect ratio will cause an increase in the wing root bending moment and increase the weight of the structure.

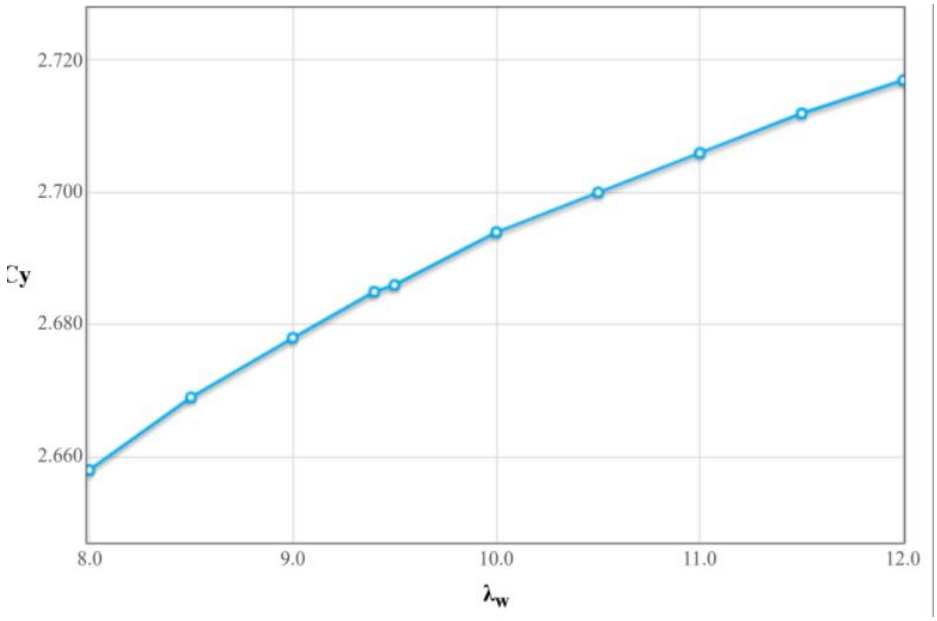

Figure 1.6 - The relationship between Take-off lift coefficient C_y with wing aspect ratio λ at wing loading of 450 daN/m^2

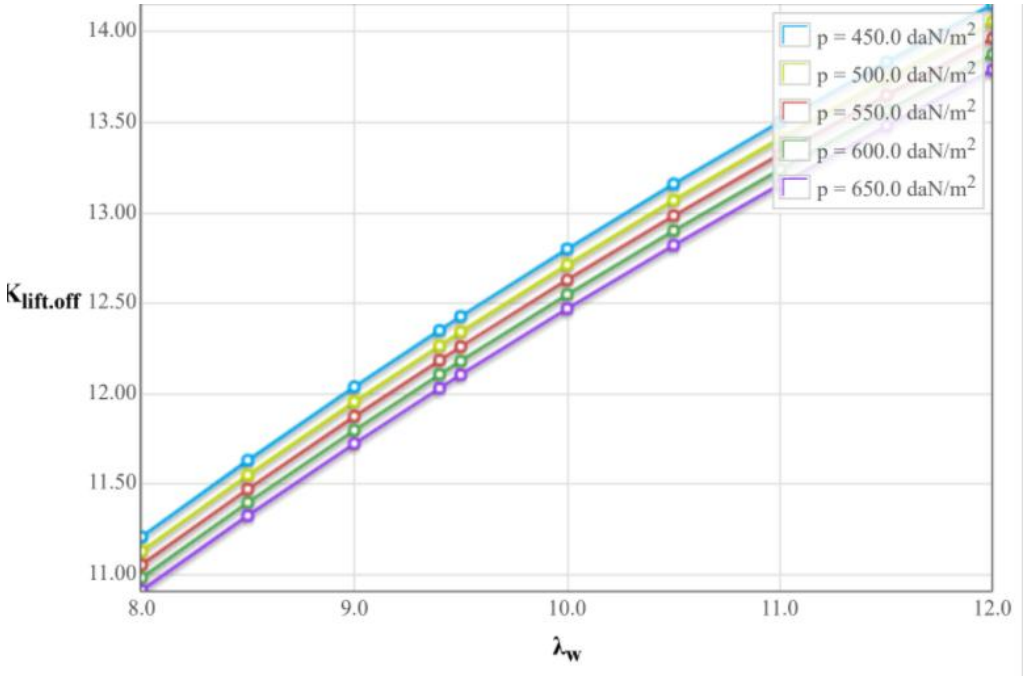

Figure 1.7 - The relationship between lift-to-drag ratio K_{t-off} and wing loading p at different wing aspect ratio λ

Component parasitic drag coefficient is equal to:

$$C_{D0} = C_f FQ(S_{wet} / S_{ref})$$

Where, C_f - component skin friction coefficient. This is a function of local Reynolds number and Mach number;

F - component form factor which is a function of the geometry;

Q - a multiplying factor (1.0~1.3) to account for local interference effects caused by the component;

S_{wet} - component wetted area;

S_{ref} - aircraft drag coefficient reference area.

Drag Coefficient of the Airplane at the Beginning of Cruising Flight is equal to 0.0927.

Induced drag coefficient is:

$$C_{Di} = (C1/C2/\pi \cdot \lambda)C_L{}^2 + (0.0004 + 0.15C_{D0})C_L{}^2$$

Where, C_1, C_2 - wing geometry factors.

After calculation, the Induce Drag Coefficient is 0.00911.

An equation of the polar curve for standard diagram is expressed:

$$C_x = C_{x0} + \frac{1+\omega}{\pi\lambda_{cr.ef}} C_L^{\ 2}$$

$$\omega = \overline{\sigma}_{b.hor.tail}(2(K_\varepsilon - 1) + \overline{\sigma}_{b.H.E}(1 - 2K_\varepsilon + \frac{\lambda_{cr.ef}}{k_{H.E}\lambda_{H.E}\overline{S}_{H.E}}))$$

And we show the result of the polar curve in figure 1.8.

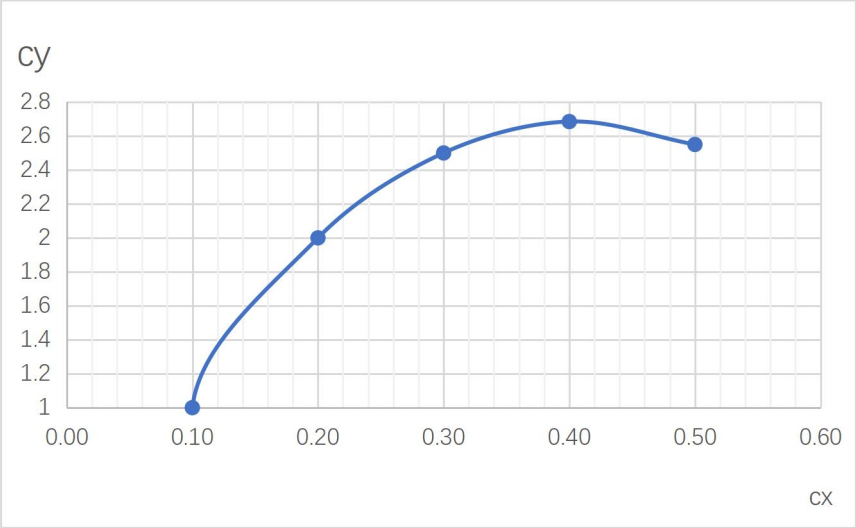

Figure 1.8 - Polar curve

1.2.2 Calculation of Performance of Takeoff

At International Standard Atmosphere (ISA) conditions H=0, ρ=1.225kg/m^3, then the minimum takeoff speed for aircraft is

$$V^2_{\min t-off} = \frac{2*10*m_0 g/10S}{1.225 C_{ymaxt\text{-}off}} = 16.33\frac{p}{C_{ymaxt\text{-}off}}$$

Speed V_2 is the speed at the end of the first phase of the takeoff in the first takeoff configuration of the aircraft (high-lift devices in the takeoff position, landing gear down):

$$V^2_2 = 1.44 V^2_{\min t-off} = 23.5\frac{p}{C_{ymaxt\text{-}off}}$$

Wing Loading p in kPa (for Gross Wing Area): At Takeoff stage, it is 5.557. Hence, the minimum takeoff speed for aircraft is equal to 210km/h. V_2 = 245km/h.

Take-off distance:

$$S_{\text{t-off}} = S_{\text{run}} + S_{\text{air}} = \frac{V^2_{t-off}/2g}{\overline{T}/W_{\text{t-off}} - \mu'} + \frac{V^2_{t-off}}{\sqrt{2}g} + \frac{h_{to}}{\gamma_{t-off}}$$

$$\mu' = \mu + 0.72 C_{D0}/C_{L\max}$$

$$\gamma_{t-off} = (T - D)/W$$

Where $\overline{T}$ is a mean value of the thrust during the takeoff run.

After calculation, the take-off distance is approximate to 1800m.

1.2.3 Calculation of Performance of Landing

The minimum landing speed for aircraft is calculated by:

$$V^2_{\text{min land}} = 16.33 \frac{p_{land}}{C_{\text{ymaxland}}}$$

The approach speed for aircraft landing is:

$$V^2_{\text{approach}} = 1.69 V^2_{\text{minland}} = 27.6 \frac{p_{land}}{C_{\text{ymaxland}}}$$

Where, P_{land} - wing loading during landing;

$$p_{land} = \frac{m_0 g(1 - \overline{m}_{fuel})}{S}$$

Wing Loading p for Gross Wing Area (kPa): At landing stage, it is 4.45. The minimum landing speed for aircraft is equal to 183 km/h. V_{approach} = 236 km/h.

Landing distance includes two parts: runway and airway. Its formular is:

$$S_{\text{landing}} = S_{\text{run}} + S_{\text{air}} = \frac{V^2_{ld}}{2\overline{a}} + \frac{1}{\overline{\gamma}}\left(\frac{V_a^{\,2} - V_{ld}^{\,2}}{2g} + h_{ld}\right)$$

Where, h_{ld} - landing height;

$\bar{\gamma}$ is a mean value of (D-T)/W;

$\bar{a}$ is the mean deceleration, taking into account an equivalent inertia time, similar to the case of the accelerate-stop distance.

After calculation, the landing distance is approximate to 1200m.

1.2.4 Conclusions

After calculation, we get the aircraft basic parameters of Aerodynamic and Flight Performance. The take-off distance is approximate to 1800m and landing distance is approximate to 1200m. The use of wingtip and composite materials make the performance of the aircraft better, compared with the prototype. And the reason why landing distance is shorten than take-off distance is that the drag coefficient is bigger. Generally, the pilot will open 30 degrees of flaps to increase drag. If necessary, it can be put full. And the thrust reverser will be open, which makes the aircraft stop quickly. It is better to do some modeling simulation to get more accurate data or even if it is possible, do wind tunnel test.

2 ECONOMICAL SELECTION

2.1 Calculation of aircraft cost and transportation cost of one ton per kilometer

The size of the loss depends on the type of aircraft. Generally, the larger, long-range aircraft are more economical to operate. But during epidemic, the operations of short/medium-aircraft are profitable compared with long-range aircraft.

The operating costs of the aircraft per flight hour consist of direct and indirect expenses. Its calculation is as follows:

$$C_{OP} = A + B$$

Where, A - direct costs per flight hour, dollars;

B - indirect costs per flight hour, dollars.

Direct expenses mainly include the fuel cost and aircraft operation, maintenance cost while indirect expenses include the airport operation, repair factories and many other costs.

The total cost of operating the aircraft for the transport of passengers per kilometer is calculated by:

$$C_{TKM} = \frac{A + B}{m_{ld} \cdot k \cdot V_c}$$

Where, m_{ld} = 22000kg = 22t, is the maximum payload of the aircraft;

V_c - aircraft speed;

K - utilization factor of the aircraft load, K= 0.65.

The size of the speed of the aircraft is determined by its cruising speed. Flight speed is the average speed of a non-stop flight, calculated considering the time spent at all stages of the flight from the start of acceleration at the airport. The formula is:

$$V_c = \frac{L \times V_{cr}}{L + (V_{cr} \times \Delta t)}$$

Where, V_{cr} - aircraft cruising speed,V_{cr} = 850 km/h;

L - non-stop flight range, L = 7200 km;

t - loss of time for waiting or maneuvering in the airport after take-off and before landing, which corresponds to a speed equal to cruising, unit in hour. t = 0.25h .

$$V_c = \frac{7200 \times 850}{7200 + (850 \times 0.25)} = 826 \text{ km}/h$$

2.1.1 Direct costs:

Direct costs of flight mainly include seven parts of expenses(unit in dollar per hour):

$$A = \sum_{i=1}^{7} A_i$$

Where, A_1 - the cost of depreciation of the aircraft;

A_2 - expenses for depreciation and overhaul of engines;

A_3 - maintenance costs of the airframe;

A_4 - maintenance costs of power plants;

A_5 - salary of flight crew ;

A_6 - fuel cost;

A_7 - other direct cost.

The cost of depreciation for one hour of aircraft:

$$A_1 = K_1 \times P_C \times \frac{1 + K_{RA} \times \left(\frac{T_C}{t_C} - 1\right)}{T_C}$$

Where, K_1 = 1.065 - coefficient considering the cost of instruction, training, flight test, etc.

P_c - price of an aircraft without engines.

$$P_C = 0.015 \cdot К_{HBO} \cdot К_{CEP} \cdot К_V \cdot m_{ep} \cdot \left(3340 + 0.077 \cdot m_{ep} - 1.05 \cdot 10^{-5} \cdot m_{ep}^{1,5}\right)$$

Where, $K_{HBO} = 1.61$

m_{ep} - the mass of an empty plane, $m_{ep} = m_{af} - m_l$.

m_{af} - the mass of the airframe, $m_{af} = 27440$ kg;

m_l - the weight of the service load of the aircraft considering the weight of the crew, $m_l = 540$ kg .

$m_{ep} = 27440 - 500 = 26900$ kg.

K_{CEP} - coefficient considering the seriality of the designed aircraft.

$$K_{CEP} = \left(\frac{35 \cdot 10^5}{m_{ep} \cdot \sum n_C}\right)^{0.4}$$

Where, $\sum n_C = 100$- the number of aircraft in a series.

$$K_{CEP} = \left(\frac{35 \times 10^5}{26900 \times 100}\right)^{0.4} = 1.11$$

K_V - coefficient taking into account the estimated flight speed of the designed aircraft

$$К_V = \frac{1}{2} \cdot \left(1 + \frac{Vcr}{800}\right) = \frac{1}{2} \times \left(1 + \frac{850}{800}\right) = 1.031$$

$$P_C = 0.015 \times 1.61 \times 1.11 \times 1.031 \times 26900 \times \left(3340 + 0.077 \times 26900 - 1.05 \times 10^{-5} \times 26900^{1.5}\right)$$

$=3988584$ \$

K_{RA} - coefficient showing the ratio of the cost of major repairs of the aircraft to the price of the aircraft.

$K_{RA} = 0.11 + (3*10^4/P_c) = 0.11 + 30000/3988584 = 0.11752$

In general, for the most of aircraft:

$T_C = 60000$ h - aircraft life time;

$t_C = 5000$ h.

$$A_1 = 1.065 \times 3988584 \times \frac{1 + 0.11752 \times \left(\frac{60000}{5000} - 1\right)}{60000} = 163\ \$/h$$

The expenses for depreciation and overhaul of engines:

$$A_2 = К_2 \cdot n_{en} \cdot P_{en} \cdot \frac{1 + К_{REN} \cdot \left(\frac{T_{en}}{t_{en}} - 1\right)}{T_{en}}$$

where K_2 = 1.07 - coefficient considering the cost of engine instruction, test, etc.

n_{en} = 2 - the number of engines installed on the aircraft;

P_{en} - the price of one engine.

$$P_{en} = 61.183 \cdot К_{HBO} \cdot N_{Emax}$$

Where, N_{Emax} = FV= 160*850/3.6= 37778 kW - maximum engine power;

K_{HBO} = 1.61

n_{en} = 2 - the number of engines installed on the aircraft;

$$P_{en} = 61.183 \times 1.61 \times 37778 = 3721308\ \$$$

K_{REN} = 0.6

In general, for the most of aircraft:

T_{en} = 6000 h - engine life time;

t_{en} = 3000 h;

$$A_2 = 1.07 \times 2 \times 3721308 \times \frac{1 + 0.6 \times \left(\frac{6000}{3000} - 1\right)}{6000} = 2024\ \$/h$$

The costs of maintenance of the airframe (A_3) and engines (A_4) consist of the costs of materials, spare components and the wages of maintenance workers. They are calculated as follows:

$$A_3 = 0.024 \cdot К_3 \cdot К_4 \cdot \left(0.39 - 0.121 \cdot 10^{-5} \cdot m_{ep}\right) \cdot m_{ep}$$

Where K_3 = 0.61 - coefficient considering the maintenance method;

$K_4 = 1$.

$$A_3 = 0.024 \times 0.61 \times \left(0.39 - 0.121 \times 10^{-5} \times 26900\right) \times 26900 = 141\ \$/h$$

$$A_4 = \frac{0.024 \cdot 16 \cdot K_2 \cdot K_5 \cdot n_{en} \cdot \sqrt{R_{max}}}{1 + 7 \cdot 10^{-5} \cdot T_{en}}$$

Where $K_2 = 1.07$ - coefficient considering non-production stages;

$K_5 = 1$- coefficient for aircraft with turbofan engine.

$R_{max} = N_{Emax} = 37780$ kW.

$$A_4 = \frac{0.024 \cdot 16 \cdot 1.07 \cdot 1 \cdot 2 \cdot \sqrt{37780}}{1 + 7 \cdot 10^{-5} \cdot 6000} = 113\ \$/h$$

The wage costs of flight crew (A_5). We consider it based on the number of passenger seats.

$$A_5 = 1.5 \cdot \left(0.9 \cdot n_{pass} - 0.00237 \cdot n_{pass}^2 - 2.9 \cdot 10^{-6} \cdot n_{pass}^3\right)$$

$$= 1.5 \times (0.9 \cdot 200 - 0.00237 \cdot 200^2 - 2.9 \cdot 10^{-6} \cdot 200^3) = 93\ \$/h$$

The fuel costs A_6 is equal to:

$$A_6 = \frac{\overline{m_T} \cdot m_0}{t_\Sigma \cdot n_{en}} \times P_k$$

Where $\overline{m_T} = 0.26$ - relative mass of fuel;

$m_0 = 98000$ kg - take-off mass of the aircraft;

$t_\Sigma = 9$ h - total flight time;

$P_k = \$\ 1.5$ / kg - the price of Jet fuel.

$$A_6 = \frac{0.26 \times 98000}{9 \times 2} \times 1.5 = 2124\ \$/h$$

Other expenses for the aircraft A_7.

$$A_7 = 0.07 \times \sum_{i=1}^{6} A_i = 0.07 \times 4758 = 333\$/h$$

Total direct costs are equal to:

$$A = \sum_{i=1}^{7} A_i = 5091\$/h$$

2.1.2 Indirect costs:

Indirect costs (B) include depreciation, maintenance of all airport facilities and the salaries of ground service workers.

Indirect costs depend on the class of the airfield and the number of take-offs and landings per hour of flight.

$$B = 0.4 \times A = 0.4 \times 5091 = 2036\ \$/h$$

The operating costs of this aircraft per flight hour are equal to:

$$C_{OP} = A + B = 5091 + 2036 = 7127\ \$/h$$

The total cost of operating the aircraft for the transportation of passengers per kilometer per ton is:

$$C_{TKM} = \frac{7127}{22 \times 0.65 \times 826} = 60.34 \times 10^{-2}\ \$/Tkm$$

The revenue received by the aviation company from operating a fleet of the aircraft on one ton per kilometer is calculated by:

$$R = \frac{P_B \times n_{pass} \times k_3}{m_{ld} \times V_c \times \tau}$$

P_B - the price of the ticket

To determine the price of a ticket, assuming that the operation of the aircraft is break-even.

$$R = C_{TKM}$$

$$P_B = \frac{m_{ld} \cdot V_c \cdot \tau \cdot C_{тким}}{n_{pass} \cdot К_з} = \frac{22 \times 826 \times 6 \times 0.6034}{200 \times 0.61} = 540\ \$$$

With a margin of 25%, ticket price: P_B = 1.25 * 540= 670 $

$$R = \frac{670 \times 200 \times 0.61}{22 \times 826 \times 6} = 75.53 \times 10^{-2}\ \$/Tkm$$

The profit earned by the aviation company per km per ton is equal to:

$$P_{rf} = R - C_{TKM} = 0.152\ \$/\text{Tkm}$$

The profit earned by the aviation company is equal to:

$$P = 0.152 \times 7200 \times 98 = 107251\ \$$$

2.2 Conclusions

One of the major expenses of airlines is the fuel cost, which is closely related to the weight and load of the aircraft. In this part, we get the operating costs of this aircraft per flight hour are 7127 $/h and the price of the ticket at $ 645. The profit earned by the aviation company is 107251$. Here we just have rough estimation.

In fact, each airline has its own set of systems. Airlines will set different rules for various situations in order to maximize their profits. In the meantime, fares and inventory of air tickets are adjusted in real time based on market feedback. There are two engines to drive technological change. One is the demand and the other one is money. It is through continuous practice operations that the aircraft designers are more targeted to improve performance.

3 SPECIAL SECTION

3.1 Development of sustainable aircraft

Asia is currently the world's largest carbon emitting region, with carbon emissions far exceeding those of other regions in the world. The main reason is that many Asian countries started large-scale economic construction after World War II, and with the rapid economic development of China, Japan, Korea, India and other countries, the demand for energy and industrial products has increased dramatically, thus driving the rapid growth of carbon emissions.

On December 16, 2021, the last A380 left the factory and was delivered to Emirates Airline, thus officially discontinuing production of the world's largest aircraft. On December 6, 2022, the last Boeing 747 left the company's factory, marking the "Queen of the Skies" Boeing 747 becomes history and announcing that the world's first wide-body four-engine civil aircraft officially ceased production.

Nowadays, sustainable aviation has become a talking point and one of the most focused areas with rapid development of the whole aviation industry, since it concerns with aviation-related emissions. New energy will have a huge impact on airports, airlines, aircraft leasing companies and manufacturers. Particularly, these years the topic of peak carbon dioxide emissions are deeply rooted among the people. During the epidemic, the global carbon emission has decreased relatively because the transportation is greatly affected. Here we can notice in figure 3.1, which shows the amount and change of global carbon emission during 2019-2022. Now the pace of development returns to that of three years ago and there are always some other factors influence the oil price, such as politics. Therefore, sustainable aircraft has definitely a big market.

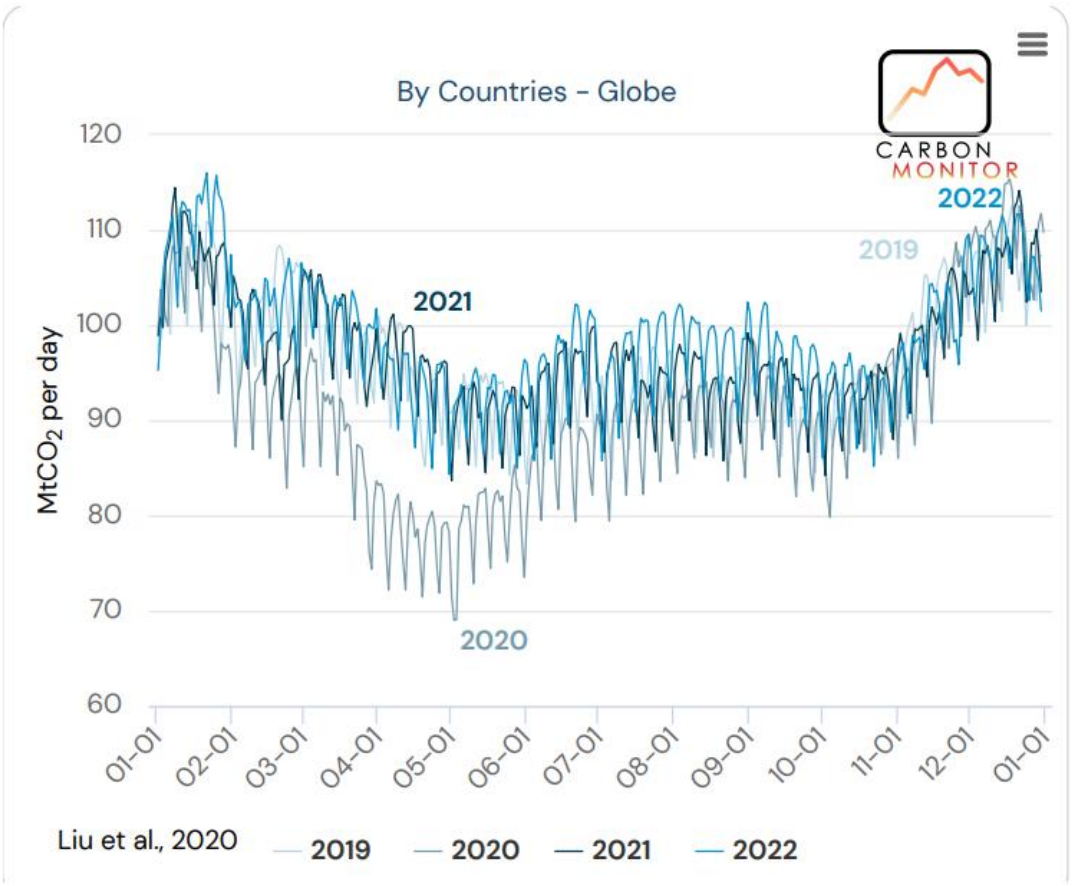

Figure 3.1 - The amount and change of global carbon emission during 2019-2022 [3]

In order to achieve the zero carbon goal, there are only two ways to go: reduce the use of fossil energy and find new energy alternatives. Hydrogen, the most abundant element in the universe, is a uniquely abundant and renewable source of energy, and its high energy density and efficiency of use make it ideally suited to our future zero-carbon needs for electricity. However, at this stage there are technical barriers. The extraction is difficult and the investment costs are very high. Another challenge in applying hydrogen to the aviation industry is its availability on a global scale and the infrastructure supply facilities.

Everything requires time to develop it. Take New Energy Vehicles as an example. In 1990, due to the lagging development of battery technology, automakers began developing hybrid vehicles under market pressure to overcome the problems of short battery and range. The global financial crisis in 2008 and the soaring international oil prices have seriously affected the energy security of all countries. At the same time, the development of new energy vehicles plays a major role in energy

security. There are many types of automotive energy sources available today, mainly gasoline, diesel, natural gas, hybrid, pure electric, and so-on. These energy sources have evolved through a history of more than 130 years of development. We likewise presume that the development of aircraft will certainly have such stage.

Though in the 21st century, there is a new breakthrough in battery technology, density, range and motor power. Small battery capacity and slow charging speed still restrict the range currently. Battery energy density and hydrogen storage system mass ratio greatly limit the range and payload of new energy aircraft. The design of electric aircraft needs long time, including the maturity of developing law enforcement, infringement and social problems such as acceptance and awareness, especially the reliability and safety of sustainable aircraft, which are critical to be overcome for pure electric aircraft to substitute for conventional propelling system [4]. The development of new energy hybrid aircraft is one of the feasible solutions to break through the current technical barriers, and several foreign aviation companies and research institutions have also chosen this option. For short and medium range aircraft, the use of hybrid electric propulsion systems can significantly save fuel and reduce noise. It is very suitable for regional passenger aircraft.

NASA studies have concluded that electrically propelled aircraft can achieve potential gains of over 60% energy savings, 90% emissions reductions and 65% noise reduction. It took the lead in 2015 in proposing a route for electric aircraft development, initiating research on three technology lines including small vertical takeoff and landing vehicles, general aviation aircraft, and large regional aircraft. The European Union sees hydrogen-powered aircraft as the only way to meet Europe's 2050 carbon emissions requirements [14].

According to energy supply method, The New energy aircrafts are mainly divided into solar aircraft, energy storage battery aircraft, hydrogen powered aircraft and biofuel aircraft.

3.1.1 Solar aircraft

The aircraft use photovoltaic cells to converts solar energy into useful electricity. China's first solar-powered aircraft, the Soarer, was

designed and built by Dr. Li Xiaoyang and Professor Zhao Yong at Beijing University of Aeronautics and Astronautics in 1992. Zephyr, solar unmanned aerial vehicle, is a High-Altitude Platform Station developed by Airbus. And the Helios, featured a futuristic solar-electric flying wing, was the success, setting a world record in altitude for any propeller driven an aerial vehicle of reaching nearly ninety-seven thousand feet [5].

On July 26, 2016, the world's largest solar-powered aircraft, SunPower 2, successfully completed mankind's first solar-powered flight around the world. It is a long-duration solar-powered aircraft that can fly continuously day and night without consuming fuel, and the energy required for flight is entirely provided by solar cells. Its wingspan reaches 72 meters, but weighs only about 2300 kg. The aircraft is equipped with more than 17,000 ultra-thin solar cells on both wings, each just 135 microns thick, equivalent to a human hair strand. With an energy conversion efficiency of 22.7%, they provide the aircraft with a peak power of 65 kilowatts during the day. A 633 kg lithium-ion battery is also installed in the engine pod, which increases its energy density to 260 Wh/kg. And it can output a stable power of 15 kW in a 24-hour cycle to overcome the night flight problem.

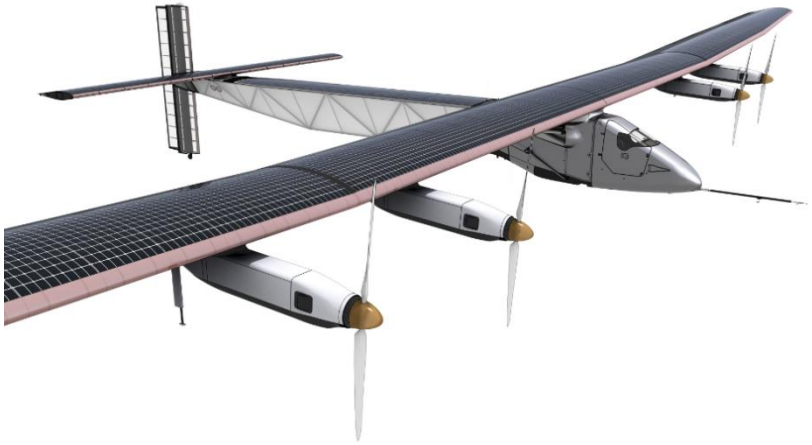

Figure 3.3 - SunPower 2

Currently due to technical limitations, the large-scale application of Solar energy in civil aviation is unlikely for the time being, only for long-endurance drones. With the unique advantages of solar energy, solar-powered drones have a wide range of uses in both the military and civilian sectors. Now many countries have started to use solar-powered drones for atmospheric research, environmental monitoring, disaster prediction, Internet services and military purposes, which brings great convenience to people's lives.

3.1.2 Energy storage battery aircraft

Nowadays, the energy storage battery aircraft mainly use lithium batteries to provide the electricity. Lithium batteries are lighter than NiCd batteries. The highest level of lithium battery at this stage has reached 400 W-h /kg and 1000 W-h /L in weight energy density and volume energy density respectively. But the power density of the motor and the energy density of the battery are insufficient for pure electric aircraft. The greater aircraft mass, the higher energy costs. Lithium batteries can provide sufficient power for small electric vertical takeoff and landing aircraft (eVTOL), such as The XPeng Voyager X2, but greater development is needed to reach commercial applications.

With the continuous emergence of new materials, lithium battery technology will continue to develop and mature. And high-capacity, high-power lithium batteries will have a broader application prospect in aviation. Now there are many electric propulsion aircraft projects in process. Here I list some representative projects from different companies.

a. X-57.

The X-57 aircraft uses 12 small motors located across the wing to increase airflow so that the wing produces lift even when the aircraft is flying slowly [6]. NASA has conducted the X-57 Maxwell Proven Aircraft program for distributed electric propulsion technology, and has completed ground high voltage and ground vibration tests. In recent years, the distributed propulsions for large-commercial-transport aircraft have been highly rewarded [7].

The X-57 demonstrator was designed with the practical needs of the urban air transportation market, including battery capacity and life, flight speed, operating economics, and urban noise. These factors may become the accepted industry norm in the future.

Figure 3.4 - X-57

b. STARC-ABL.

The STARC-ABL, a 150-passenger class commercial transport with a traditional "tube-and-wing"shape, is under development by ASAB aims to bridge the gap between current jet fuel-powered aircraft and future all-electric vehicles [8]. NASA has conducted STARC-ABL hybrid aircraft research for Boeing 737 volume aircraft, with a 2.6 MW electric motor embedded in the tail and attached surface layer suction technology, which is expected to reduce drag by 7 to 12 percent.

Figure 3.5 - STARC-ABL

c. ACCEL.

Accelerating the Electrification of Flight (ACCEL) is one of the world's fastest all-electric aircraft, reached up to 480km/h. Rolls-Royce

presents its "Strategic Development Plan for Electric Propulsion Aircraft in the 21st Century" in 2019. ACCEL project intends to pioneer a third wave of aviation in support of Rolls-Royc's strategy to champion electrification [9]. In September 2021, the Rollo electric aircraft made its maiden flight. Compared with conventional aircraft, its tail-sitter layout is uncommon since there are over 6,000 batteries installed in the front section of the nose to drive the propulsion system, shown in figure 3.6.

Figure 3.6 - ACCEL

d. RX4E.

The four-seat electric RX4E aircraft is a new energy general aviation product developed by LiaoNing General Aviation Research Institute. The aircraft has extensive use of carbon fiber composites for structures to decrease weight, with a range of 1.5 hours and range up to 300 km. The electric propulsion system used by the aircraft is the first application of residual electric drive technology in the field of general aviation in China.

The total installed capacity of the system's power battery is nearly 70kWh. And its electric cell is China's first commercially applied electric cell product with an energy density of over 300Wh/kg, which is at the leading level internationally. It can be applied to short-haul transportation, pilot training, sightseeing trips, aerial photography and other fields.

Figure 3.7 - RX4E

3.1.3 Hydrogen-powered aircraft

Since 2008, Airbus has been testing hydrogen and oxygen-based fuel cell systems on its A320 aircraft, and has been quite "dedicated" to hydrogen energy. The ZEROe new energy aircraft will be delivered in 2035. While Boeing is also promoting hydrogen power research, it has paid more attention to the development potential of hybrid power. In March 2022, the UK's Aerospace Technology Institute (ATI) unveiled its final proposal for three hydrogen-powered aircraft concepts called FlyZero, covering regional jets, narrow-body trunk airliners and mid-size airliners. ATI also said that the future hydrogen aircraft has the potential to cover 100% of short-haul flights and 93% of existing long-haul flights [10].

As a fuel, Hydrogen has a high calorific value (140.4MJ/kg), which is 3-4 times higher than the calorific value of fossil fuels such as gasoline of the same mass. Compared with electric propulsion, liquid hydrogen has a higher energy density in terms of weight and volume and can be applied to medium to large trunk or regional airlines. It is a colorless, odorless, high-energy liquid fuel with a saturation temperature of about 20K and a saturation density of about 70.8 kg/m^3 at one barometric pressure. In theory, liquid hydrogen can cool the entire electric drivetrain to superconducting temperatures, at which point resistance will disappear from the system and efficiency rises rapidly.

In general, there are two approaches to using hydrogen as a power source for aircraft propulsion. The first one is by burning hydrogen instead of jet fuel in a traditional turbofan or turboprop combustion

engine. Improve the design of conventional turbine engines, including combustion chambers, fuel systems and control systems to form new power system.

And the other one is by using a fuel cell to achieve the "hydrogen-electricity" conversion. The hydrogen fuel cell uses onboard hydrogen storage and oxygen in the air to generate direct current, which is converted to alternating current by an inverter. And the motor drives a reduction gear which in turn drives a fan to generate power. Currently, the main technical barrier to hydrogen turbine power is in the mechanical field, while the main technical barrier to hydrogen fuel cell power is in the chemical and electrical fields.

Here I list few large projects which devoted to develop hydrogen-powered aircraft.

a. ZEROe.

Airbus has announced three concepts for a global zero-emissions civil aircraft scheduled to enter service in 2035. Each of these concept aircraft represents a different approach to zero-emissions flight, exploring various technical pathways and aerodynamic configurations. All three ZEROe concepts are hybrid-hydrogen aircraft, which powered by hydrogen combustion through modified gas turbine engines [11].

The first option shown in figure 3.8, uses turbofan engines, carries 120-200 passengers with a range of more than 2000 nautical miles. And it is capable of transcontinental operations and powered by modified gas turbine engines. The liquid hydrogen will be stored and delivered through tanks located behind the rear pressure-resistant bulkhead.

Figure 3.8 - ZEROe with turbofan engines [11]

The second option, shown in figure 3.9, uses turboprop engines instead of turbofan engines for a range of more than 1000 nautical, carrying up to 100 passengers which makes it ideal for short trips. The aircraft is propelled by two hybrid hydrogen turboprop engines driving eight propellers, and its liquid hydrogen storage and distribution system are also located behind the pressure bulkhead. In order to arrange the large diameter propeller and adapt to the harsh environment of the runway, this plan adopts the layout of "upper monoplane + T-tail".

Figure 3.9 - ZEROe with turboprop engines

The third option is a ‘Blended-Wing Body’ (BWB) design, carrying up to 200 passengers. The BWB design has a range of more than 2000 nautical miles. As shown in figure 3.10, the extra-wide fuselage provides a variety of options for hydrogen storage and delivery, as well as cabin layout. Its liquid hydrogen storage tank is stored under the wing.

Figure 3.10 - ZEROe Blended-Wing Body design

b. Dash-8 300.

The Dash8 series is a twin-engine turboprop regional aircraft developed by the original Canadian company de Havilland. The engine on the right side of this aircraft was modified to use hydrogen fuel, while the left side still uses the traditional propeller engine for safety. And it uses Plug Power's fuel cell and magniX's electric motor, loaded with 30 kg of liquid hydrogen and multiple sensors.

The company uses modular capsules to store hydrogen and load it directly onto the aircraft as a fuel tank. The aircraft has completed its first taxi test and is expected to fly to the sky in 2023. We notice that there is few words ‘universal hydrogen’ on the right engine in figure 3.11.

Figure 3.11 - Dash-8 300

c. FZN-1E.

The FlyZero project aims to achieve zero carbon emissions from commercial aviation by 2030. Among three concepts, the narrow-body concept is based on the A320neo, targeted at a design range of 4445 km and a seating capacity of 180. The fuselage of the FZN-1E is ten meters longer and almost a meter wider than that of the A320neo, and the wingspan is 39.3 meters compared to 35.8 for the A320neo [12].

From the figure 3.12, we can notice that this concept has a different wing design (no fuel storage, all fuel is stored in the fuselage) with folding wingtips and the aft width of the aircraft is increasing, shaping a tapering fuselage, in order to provide wider space at the rear for the fuel tanks. And two hydrogen-burning turbofan engines are mounted under a T-tail which facilitate the transmission of hydrogen for engines. The variable cross-section could "encourage natural laminar flow" to reduce drag. Besides, the "duck wing" in the nose position solves the problem of center of gravity shift under different flight and load conditions. It provides better longitudinal leveling capability and pitch performance.

Figure 3.12 - FZN-1E

3.1.4 Biofuel aircraft

It is a new energy aircraft with a structure and system that most closely resembles a conventional aircraft, using biofuel as an energy source. Aviation biofuels have a wide range of raw materials, including algae, oilseed crops, waste oil and agricultural waste. For example, Seaweed, an important biofuel, can reach carbon balance as the carbon dioxide absorbed during its growth is basically equal to the carbon dioxide released during combustion.

In 2012, Boeing and COMAC developed aviation biofuel and CO_2 reduction technologies using waste cooking oil as fuel. In August 2012, China Petrochemicals and Airbus signed the China Eastern Airlines Biofuel Development Agreement to start research on the development of new biofuels [13]. In collaboration with Boeing and other members, Neste has come up with a fuel called “Drop-in” that can be used in jet and turboprop engines. The fuel has been successfully tested in 1,200 commercial aircraft. On November 21, 2017, Hainan Airlines flight HU497 took off from Beijing Capital International Airport to Chicago and arrived in the United States after a flight of about 12 hours. The aircraft used 15% bio-kerosene converted from "gutter oil".

Compared to traditional fossil fuels, biofuels have significant environmental advantages, reducing carbon emissions by more than 35% compared to equivalent fossil fuels. However, there are still many

uncertainties about its promotion in China. The biggest obstacles are the high price and insufficient production.

After listing four different types and comparison, we show that the intrinsic parameter of fuel and the current parameters of the battery and engine in the table 3.1.

Table 3.1 - Parameters of new energy power system and the traditional power system [14]

Fuel	**Caloricity, J/kg**	**Volumetric Energy Density, kWh/L**	**Mass energy density, kWh/kg**
jet fuel	0.4*10^8	8.9	12
liquid hydrogen	1.4*10^8	2.76	38.9
Battery	**power density, kW/kg**	**energy density, Wh/kg**	
hydrogen cell	0.75	-	
lithium-ion battery	3.5	250	
Engine	**power density, kW/kg**	**unit-power, kW**	**Gross efficiency, %**
conventional turbine engines	6	-	42
hydrogen turbine engine	4.5	-	35
superconducting motor	4	250	-

3.2 Review of hydrogen storage

Airbus believes that a powertrain could reduce the weight of the aircraft by half and its electrical losses by half. China's new energy

aviation development take hydrogen fuel hybrid regional aircraft as an entry point, gradually transition to larger size hydrogen turbine regional/mainline aircraft, and realize a completely independent new energy aircraft industry chain covering all markets and product lines around 2050 [14]. The application of liquid hydrogen in aviation is still being explored. Due to the low temperature and low boiling point, the leakage of liquid hydrogen may lead to serious safety accidents. On the one hand, the low-temperature characteristic of liquid hydrogen may cause greater harm to the surrounding equipment and personnel. On the other hand, the gaseous hydrogen formed after the evaporation of liquid hydrogen is highly prone to explosion when mixed with air. In addition, hydrogen may also cause problems such as hydrogen embrittlement and hydrogen corrosion. For storage tank design, hydrogen production technology, safety assurance and ultra-low temperature applications are currently the challenges faced by researchers. Therefore, the storage container is very critical to ensure the safe and economic application of hydrogen. After the technology matures, hydrogen-fueled aircraft can also fly long distances in the future.

Since hydrogen fuel is very different from traditional petroleum fuel, for airports, how to realize the transportation and storage of hydrogen fuel at low cost will directly affect the future operation of airlines. Current research indicates that liquid hydrogen storage tanks should be spherical or columnar in shape, and conventional wing tanks are not suitable for storing liquid hydrogen fuel. Therefore, for short and medium range passenger aircraft, the existing airframe structure needs to be adapted or redesigned [15]. Large liquid hydrogen tanks are generally spherical in shape to reduce heat leakage and the evaporation rate of large storage tank is much lower than that of small storage tank. In order to achieve efficient utilization of the internal space structure of the aircraft, Large-scale hydrogen energy storage in aircraft requires the introduction of revolutionary aircraft design concepts, such as wing-fuselage fusion design and boxed wing structure.

The U.S Department of Energy requires commercial hydrogen storage densities of 6.5 wt% by mass (mass of stored hydrogen as a percentage of the total hydrogen storage system) and 62 kg/m^3 by volume [16]. Hydrogen storage technology is divided into two directions: physical hydrogen storage and chemical hydrogen storage.

Physical hydrogen storage mainly includes normal temperature and

high-pressure hydrogen storage, low temperature and liquefaction hydrogen storage, low temperature and high-pressure hydrogen storage and porous material adsorption hydrogen storage; chemical hydrogen storage mainly includes metal hydride hydrogen storage and organic liquid hydrogen storage. Several typical hydrogen storage technology performances are shown in Table 3.2.

Table 3.2 - Comparison of typical hydrogen storage technology [17-20]

	High pressure gaseous hydrogen storage	Low temperature liquid hydrogen storage	Solid state hydrogen storage	Organic liquid hydrogen storage
Hydrogen storage density (%)	1.0~5.2	5.1~10	1.0~10.5	5.0~10.0
Volumetric hydrogen storage Density (g/L)	25~35	71	35~80	40~45
Mass fraction (%)	6	30	11	-
Temperature (°C)	15	-253	15	15
Pressure (MPa)	20	0.5	0.4~10	0.013
Advantages	Easy operation, low cost	High hydrogen storage density and purity	High hydrogen storage density, purity and high safety	High hydrogen storage density and high safety

High-pressure gaseous hydrogen storage means that at a certain temperature and volume, the pressure of the system is increased and the hydrogen is compressed in a high-pressure hydrogen storage tank, which is often used for automotive hydrogen storage. It is convenient and

commercially available. However, the low density of hydrogen storage and potential safety risks make it not the preferred solution for long-term hydrogen storage technology. It is the most common method of hydrogen storage in current hydrogen energy vehicles rather than in aviation industry. At present, this type of hydrogen storage and transportation methods are mainly in long tube trailers, which are equipped with perfect safety devices and detailed operation specifications from filling to transportation. In addition, there are also synchronized protection measures in the field of over-temperature alarm, fire protection, over-pressure protection, over-current protection and hydrogen leakage monitoring to ensure safety. This technology is quite mature now.

Solid state hydrogen storage refers to the use of hydrogen storage materials such as metal hydrides that can reversible hydrogen absorption and discharge properties. Solid state hydrogen storage includes both hydride and adsorbent forms of hydrogen storage. It has low density by weight, but high density by volume, good safety and high purity, which is still in the development stage. It is an important direction for future development.

Low temperature liquid hydrogen storage means that hydrogen is stored in an adiabatic vessel at atmospheric pressure, at a temperature of -253 °C, where the hydrogen is changed from a gaseous state to a liquid state. It requires liquefied hydrogen storage, which can significantly increase the hydrogen storage density. However, the energy consumption and cost of liquid hydrogen storage is high, and it is currently used in the aerospace and aviation industry.

Research related to hydrogen energy storage and transportation technology and hydrogen fuel cell technology will reach saturation around 2027, and research related to hydrogen energy production technology will reach saturation around 2031 [21]. Airbus has established Zero Emission Development Centers (ZEDC) in Spain, France, Germany and the UK to develop hydrogen energy technologies, has built the first on-board liquid hydrogen storage tanks and is preparing to use the TJ-100 turbojet engine to study the effects of hydrogen combustion on wake characteristics.

Above all, for this part, I am willing to do some work about the liquid hydrogen storage tank in aviation to facilitate the use of hydrogen aircraft and the progress of the energy transition.

In this paper, the left fuel engine of the aircraft is directly replaced by a hydrogen turbine engine, which has relatively low technical difficulty and development cost. Besides, it provides a sound foundation for the development of pure hydrogen-powered aircraft later.

3.3 Theoretical Background of liquid hydrogen storage

With regard to standards for the storage and transportation of liquid hydrogen, the International Organization for Standardization (ISO) are:

Liquid hydrogen-land vehicle fuel tanks (ISO 13985:2006);

Basic considerations for the safety of hydrogen systems (ISO 15916-2015).

American Institute of Aeronautics and Astronautics (AIAA) states the Standardization 'Guide to safety of hydrogen and hydrogen systems' (AIAA-G-095A-2017). On December 9, 2020, the International Organization for Standardization Technical Committee on Hydrogen Energy discussed and adopted a standard proposal for liquid hydrogen, PWI 24077 (LH2 use in non-industrial settings), which focuses on the safety of the use of liquid hydrogen and the first issue raised in the proposal is the high risk of the use of liquid hydrogen [22].

In china, the standards for liquid hydrogen storage are:

Technical requirements for storage and transportation of liquid hydrogen (GB/T 40060-2021);

Liquid hydrogen storage process and facilities (GB50156-2021).

Pressure vessel analysis and design methods are usually divided into three categories: stress classification method, limit load analysis method and elastic-plastic stress analysis method. Stress classification method refers to the method combined with the elastic stress analysis and plastic design guidelines. The main difference between the limit load analysis method and the elastic-plastic stress analysis method is that the former only uses the yield limit of the material, while the latter needs to use the actual stress-strain curve including the strain-hardening effect of the material.

In engineering applications, elastic analysis is often used instead of plastic analysis. The damage of the actual structure is a gradual process.

As the load increases, the high stress area firstly enters into yielding, and the plastic area becomes larger as the load continues to increase, while the stress is redistributed. When the load reaches a limit load, the deformation will increase and the overall plastic deformation will occur even if the load is no longer increased. Compared with the stress classification method, the ultimate load analysis method not only avoids the difficulties of stress classification, but also reflect the failure process of the pressure vessel under load more realistically, and it gives a more accurate assessment of the prevention of plastic collapse in the prevention of plastic collapse failure [23].

a. Stress classification method.

In ASME VIII-2, the stress classification method classifies stresses into primary P_m (acting on the overall structure, caused by mechanical loads), primary overall film stress P_L (acting on the local area, caused by discontinuities in the overall structure), primary bending stress P_b (acting on the overall structure, caused by mechanical loads, distributed linearly along the cross-section), secondary stress Q and peak stress F.

This part of the design divides them into three categories, primary stress P, secondary stress Q and peak stress F. Primary stresses are caused by external loads, balancing mechanical loads and maintaining structural equilibrium. Secondary stress is the stress necessary to meet external constraints, and is the bending stress caused by the overall structural discontinuity. The peak stress is the stress increment attached to the primary and secondary stresses, caused by the local structural deformation discontinuity, which does not cause significant structural deformation, but will lead to fatigue [28].

In practice, the stresses or combinations of these stresses are evaluated according to different permissible stress limits, otherwise the design of the structure can lead to catastrophic consequences.

Design load limit:

$$S_1 = P_m \le KS_m$$

$$S_2 = P_l \le 1.5KS_m$$

$$S_3 = P_l + P_b \le 1.5KS_m$$

$$S_4 = P_l + P_b + Q \le 3S_m$$

$$S_5 = P_l + P_b + Q + F \le S_a$$

Operating load limit:

$$P_m \le S_{mt}$$

$$P_l + P_b \le KS_m$$

Where S_m - Minimum stress value at the special temperature (Material design stress strength), S_{mt} - the permissible limit of overall primary film stress, determined at the maximum average wall temperature for a given load condition, K - Load combination factor, S_a - the allowable peak stress intensity value obtained from the fatigue curve.

S_m is obtained by dividing the short-time tensile properties of the material(R_{el}, R_m, R_{el}^t) by the corresponding safety factor (n_b, n_s, n_s^t). According to Chinese industry standard JB 4732-95, generally, for steel material, n_b=2.6, n_s=1.5, n_s^t=1.5.

$$S_m = \min\{\frac{R_{el}}{n_s}, \frac{R_m}{n_b}, \frac{R^t{}_{el}}{n^t{}_s}\}$$

In the finite element computational analysis, only the results of the calculation of the total stresses at various places in the structure can be given, and there is disagreement about the further division of the film + bending stresses obtained by the equivalent linearized stress treatment. Although some experts have proposed other methods, the complexity and uncertainty of the design process are increased.

b. Limit load analysis method.

The limit load analysis method is an alternative to the stress classification method, which can be used to obtain a more accurate judgment. When the requirements of limit analysis are met, there is no need to assess the primary stresses. Limit load analysis involves the failure mode of plastic damage and the beginning of the overall plastic deformation of the structure and it is applicable to single or multiple static loads applied in any prescribed sequence [24]. The process of it is shown in figure 3.13.

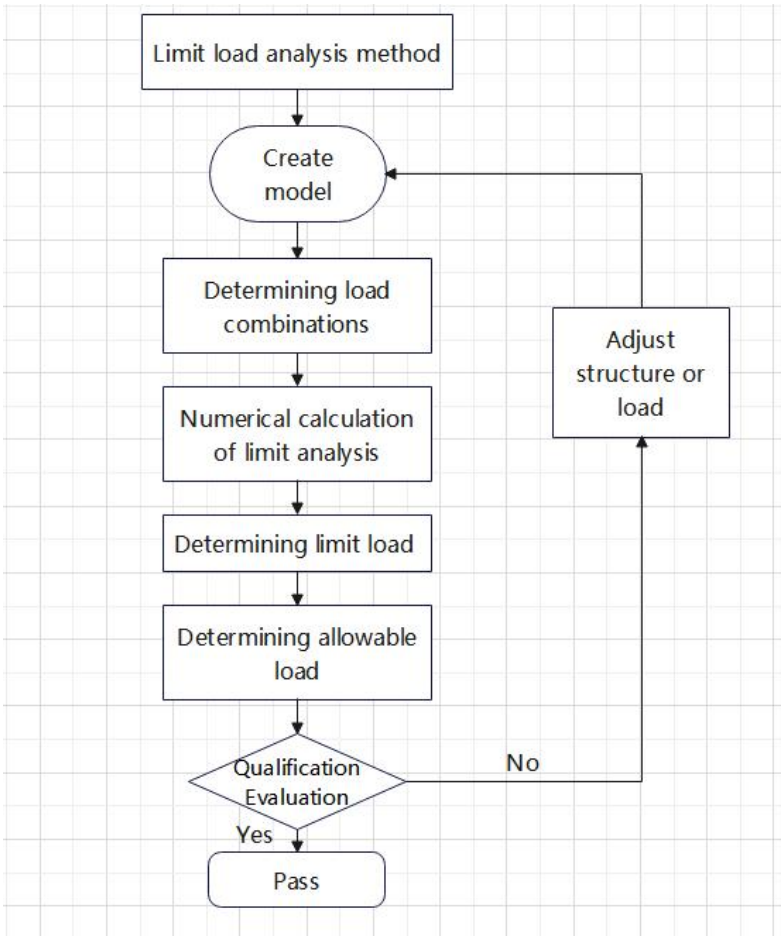

Figure 3.13 - The process of Limit load analysis method

Several important conditions involved for finite element numerical model are described here. The limit load analysis method uses an ideal elastic-plastic material model with small displacement theory. Namely the geometric change effect caused by deformation is not considered. Besides, it applies the finite element method and the associated flow law to find the limit load that causes the collapse of the overall structure. The associated flow criterion requires that the yield surface is smooth, which the points on the yield surface have a unique normal direction.

The allowable load of the element is determined by introducing a safety factor or by using the design concept of load resistance factor.

c. Elastic-plastic stress analysis method.

The theoretical basis of the elastic-plastic analysis method is the incremental plasticity theory. It uses the strain-displacement nonlinear

relationship for large deformations, the Von-Mises yield criterion and the associated flow law applicable to most metallic materials, which is similar to the method of limit load analysis. Considering the load conditions and deformation characteristics of the structure, the failure load is calculated by elasto-plastic analysis, to which a design factor is applied to determine the allowable load of the structure. For example, components that show a decrease in stiffness with deformation need use this method. The basic process is parallel to limit load analysis method, except the numerical calculation.

In the finite element numerical solution, we can get the real stress-strain curve of the material by constructing a stress-strain model when the yield strength, tensile strength, elastic modulus and post-break elongation of the material are known. Then it will be used for the solution of the elastic-plastic analysis.

3.4 Analysis of Airborne liquid hydrogen cylinder ultimate load capacity

The inner cylinder is mainly used for low-temperature liquid hydrogen, which is chemically flammable and explosive. The volume will change rapidly when the liquid state is heated to gaseous state and it will lead to a rapid increase in internal pressure.

3.4.1 Structure:

The structure is mainly divided into cylinder outer container, inner container, liquid level sensor, insulation layer, hydrogen system cold box, cylinder connection and transportation system.

The inner vessel of the liquid hydrogen storage tank is equipped with a safety valve, and the outer vessel is equipped with an over-pressure relief device. There is a shut-off valve between safety valve and storage tank. Apart from maintaining a vacuum between inner container and outer container, there is also an insulation layer composed of insulation material to reduce radiative heat transfer. Inner packer the maximum release pressure of the safety valve should not be larger than $1.1P_0$. Low temperature hydrogen and cold leakage may cause icing of

piping, valves and other components, leading to material rupture or failure of components, especially safety devices. Here we do not consider the connection of the inner and outer container components (pipe, support systems) and the injection and discharge of cryogenic liquid hydrogen and gases, recycling systems, etc.

Large stationary tanks are generally spherical in shape, but they occupy a large area and are difficult to support and transport, while small and medium-sized liquid hydrogen storage tanks generally use vertical or horizontal cylinder. Here we use the type of horizontal cylinder. In order to ensure that no relative displacement and structural deformation occur during the transportation, the inner cylinder and outer cylinder are supported by an axial combination, which is one end fixed and one end sliding. The rear end of the cylinder can be moved freely in the axial direction by the support structure.

The schematic diagram of the liquid hydrogen cylinder structure is shown in Figure 3.14.

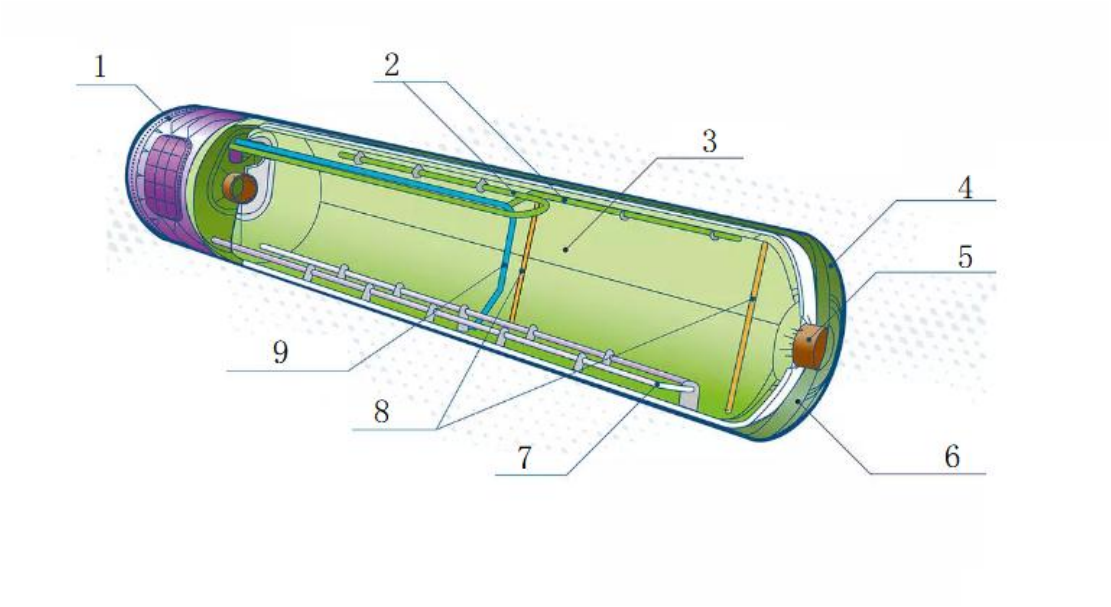

1. hydrogen system cold box and cylinder connection system; 2. gas extraction pipe; 3. inner container sensor; 4. outer container; 5. suspension mount; 6. insulation layer; 7. heater pipe; 8. liquid level probe; 9. liquid refuel or extraction pipe

Figure 3.14 - The schematic diagram of the liquid hydrogen cylinder structure [25]

3.4.2 Material selection:

The selection of materials for liquid hydrogen storage and transportation containers needs to focus on the adaptability of metal materials in the liquid hydrogen environment, hydrogen embrittlement, the low temperature mechanical properties of the material, the thermal properties of the liquid hydrogen temperature zone, etc [26].

The chemical composition of a material plays a very important role in its performance, and nickel is an significant element in improving the low-temperature toughness of steel. Gloyer Taylor Laboratories (GTL) is developing a composite cryogenic tank that can store more liquid hydrogen in a lighter tank weight, including composite tanks, skirts and vacuum insulated bottle shells.

The inner container is usually made of metal and composite materials. At present, the international liquid hydrogen storage and ground transportation containers usually choose austenitic stainless steel as the main material of the container, such as 304L, 316L, 321, 347 type. Austenitic stainless steel has high strength, good low temperature toughness, excellent corrosion resistance, forming properties and welding properties [27]. At low temperatures, the thermal conductivity and specific heat capacity also decrease, reducing the heat loss of the vessel.

When injecting or discharging liquid hydrogen, the tank may be subjected to cyclic stresses due to temperature changes or inertia forces during transport. Therefore, we need to consider the material fatigue life. Compared with austenitic stainless steel, aluminum alloy has obvious advantages in light weight, formability, weldability, corrosion resistance. Nowadays, Aluminum alloy has been used in the aerospace field for liquid hydrogen storage tanks.

Considering that the material data are confidential at liquid hydrogen temperature, the known data at different temperatures are used for conversion in this paper. Here I list the properties of 316L and A5083 at temperature of 20K, shown in table 3.3. The density of a solid or liquid substance changes only slightly when the temperature and pressure change. Here we assume its density remains constant.

Table 3.3 - Properties of material used for liquid hydrogen storage [28-29]

	Austenitic stainless steel 316L	Aluminum alloy A5083
Tensile Strength σ_b (MPa)	621	520
Yield strength $\sigma_{0.2}$ (MPa)	333	270
Elongation after fracture(%)	58	30
Density (g/cm^3)	7.98	2.68
Young modulus (Gpa)	213	80
Poisson ratio	0.3	0.32

In this part, considering the performance of each material and product cost comprehensively, we use the Aluminum alloy A5083 as the material of liquid hydrogen cylinder container. The detailed calculations for two materials are shown in part 4.3.4.

The outer container of the liquid hydrogen cylinder is not in direct contact with the liquid hydrogen. But high strength and low density are required. Carbon steel is generally used for the outer container. The performance of S32168 and S30408 material is shown in Table 3.4. Here the cylinder shell material is selected as S30408.

Table 3.4 - The performance of S32168 and S30408

Performance	S32168	S30408
Density (g/cm3)	8.03	7.93
Tensile Strength σ_b (MPa)	520	520
Yield strength $\sigma_{0.2}$ (MPa)	205	210

End of table 3.4

Elongation after fracture(%)	40	40
Modulus of Elasticity (Gpa)	193	207

Liquid hydrogen does not oxidize at ultra-low temperatures. And the main loss is evaporation, which is the most important concern in liquid hydrogen storage. The insulation material conforms to the provisions of the current national standards GB/T 31480 and GB/T 31481, and meets the requirements for use under the conditions of liquid hydrogen. There exists a wide range of insulation materials to choose to minimize heat transferring. Here are some insulation materials shown in table 3.5.

Table 3.5 - The performance of insulation materials [30]

Material	high vacuum heat conductivity coefficient ($\times10^{-3}W\cdot m^{-1}\cdot K^{-1}$)	volume density (kg/m^3)	shape
Spray-On Foam	7.8	42	spray
Multi-layer insulation (MLI)	<0.1	45	felt
Aerogel Beads	1.5	133	felt
Layered compound insulation (LCI)	0.1	50	felt
Glass wool	1.9	16	felt

The liquid hydrogen storage tank adopts the insulation form of Multi-layer insulation since its properties of low thermal conductivity, low radiation, high thermal insulation and light weight. Its cross section is shown in figure 3.15.

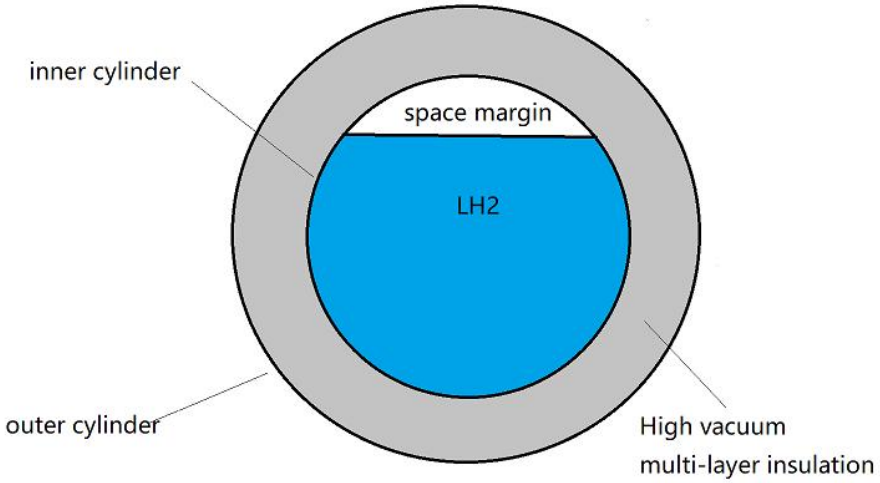

Figure 3.15 - The cross section of the liquid hydrogen cylinder

As the shell of the liquid hydrogen cylinder material is austenitic steel, in order to meet the strength and toughness requirements and reduce the harmful impurities at the welded joints, the welding material of the steel used is A107.

3.4.3 Parameters of liquid hydrogen cylinder:

The fuel consumption of A321 neo can go up to about 2.3 tons per hour. So one engine's fuel consumption is about 1.2 tons. One kilogram of hydrogen is equivalent to 3 kilograms of kerosene. 7 tons of aviation kerosene is equivalent to 2.3 tons of hydrogen. The density of liquid hydrogen is nearly 71 kg/m^3.

$$2300 \div 71 \approx 32\text{m}^3$$

In addition, due to thermal stratification and overfilling phenomenon, the storage tank can not be filled too full. Generally, a 10% margin of space should be left.

$$32 \div (1 - 0.1) \approx 36\text{m}^3$$

Therefore, for one engine of the aircraft whose flight schedule last 6 hours, its volume needs at least 36m^3.

Since liquid hydrogen storage usually has a working pressure of 0.4MPa or less, the inner chamber needs to have a certain pressure-

bearing capacity, usually over 1MPa.

The cylinder is a horizontal structure with a volume of 36m^3 and a design pressure of 1MPa.

The inner diameter of the outer bile cylinder is 3m, the thickness of the cylinder is 6mm, and the length of the cylinder is 5.1m.

The outer diameter of the outer bile cylinder is 3.1m, the thickness of the cylinder is 9mm, and the length of the cylinder is 5.3m.

3.4.4 Theoretical calculation of inner container load bearing:

The thickness of the cylinder does not exceed half of the inner radius. According to ASME VIII (Pressure vessel specification analysis) section 1, the formula for calculating the inner wall thickness as determined by the inner diameter is

$$t = \frac{PR}{SE - 0.6P}$$

Where, S - the Permissible stress of the material used at the design temperature, MPa;

S=δ_s/n=500/1.6=313MPa

E - Longitudinal welded joint coefficient;

R - radius of inner cylinder, mm.

$$t = \frac{1*1500}{0.85*313 - 0.6*1} = 5.65\,\text{mm}$$

China's standard GB250-2011 standardizes the design of steel pressure vessels. Mid-diameter formula form is simple and easy to calculate and it is commonly used in the design of thin-walled steel vessels. We can calculate its bursting pressure P_b by the formulation:

$$P_b = 2R_m \frac{K-1}{K+1}$$

Where, R_m - the Tensile Strength of the material, MPa;

K - the ratio of outer diameter to inner diameter;

K=3000/2988=1.004

R - radius of inner cylinder.

If use Aluminum alloy A5083, the maxium bursting pressure is:

$$P_b = 2 \times 520 \times \frac{1.004 - 1}{1.004 + 1} = 2.08 MPa$$

If use Austenitic stainless steel 316L, the maxium bursting pressure is:

$$P_b = 2 \times 621 \times \frac{1.004 - 1}{1.004 + 1} = 2.48 MPa$$

Though the bursting pressure of 316L is bigger than A5083, consideirng the density of A5083 is much less than 316L, here A5083 meets the requirment.

$$P_b = 2.08 MPa > 1 MPa$$

And 6mm > 5.65mm, thus the thickness of the inner cylinder 6mm is good enough.

3.4.5 Modeling and simulation:

After the calculation of its basic parameters and the choose of material, we build the model of the inner container. Here we do not consider its pipe system in order to simplify the issue.

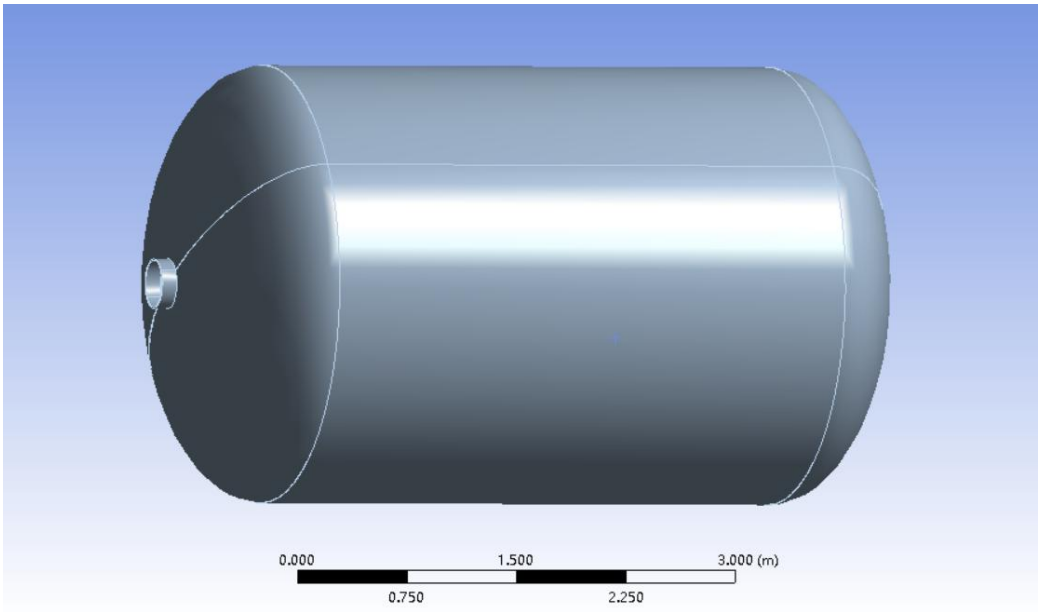

Figure 3.16 - The model drawing of the liquid hydrogen inner cylinder

Then we set the model material with A5083. We choose the method of Tetrahedrons as the mesh method, which has good adaptability to

complex geometry and quickness to generate meshes. The mesh condtion is shown in figure 3.17.

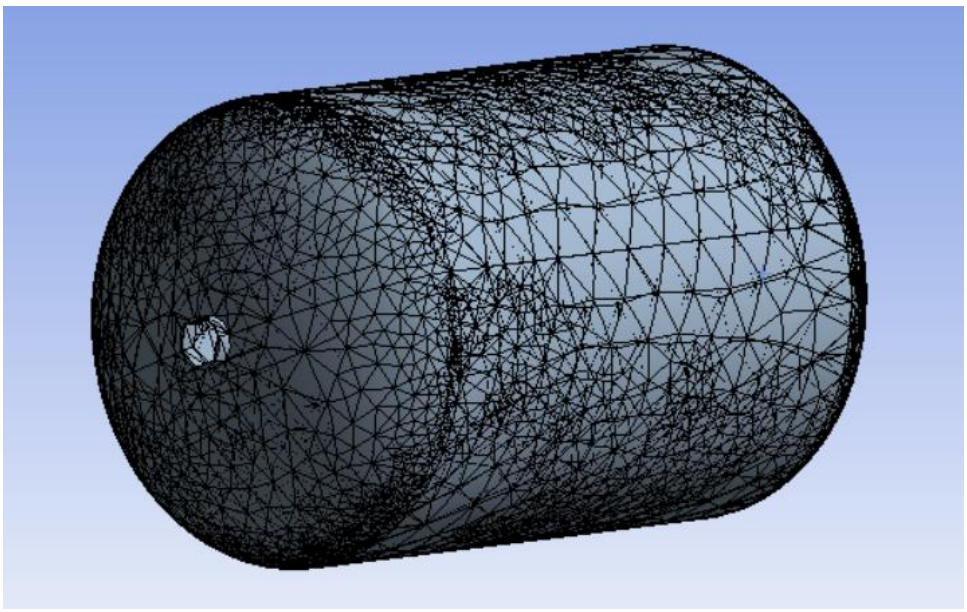

Figure 3.17 - The mesh condition of the model

The inner container is fixed by both ends. And we apply 0.4MPa pressure to simulate its work condition.

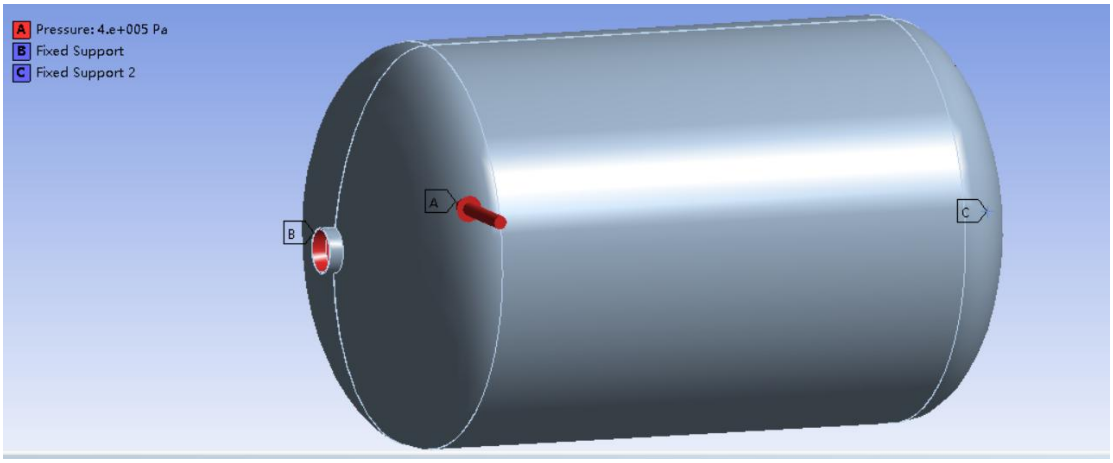

Figure 3.18 - The structural setting of the model

After all the preparation steps, we do the ‘solve’ and the results are shown. The plastic strain of the cylinder is 0. In Workbench, the large deformation switch is turned on to take into account the stiffness changes caused by cell displacement and deformation, and the new stiffness matrix is regenerated with each iteration, which is more accurate but also

adds a certain amount of calculation. In this part, we turn on the large deflection and use elasto-plastic analysis method to do the the numerical calculation. The difference between different conditions are shown in figure 3.19. According to the calculation result, the maximum stress value is 143.81 MPa, while the yield stress of A5083 is 520 MPa. Therefore, the inner container meets the requirements.

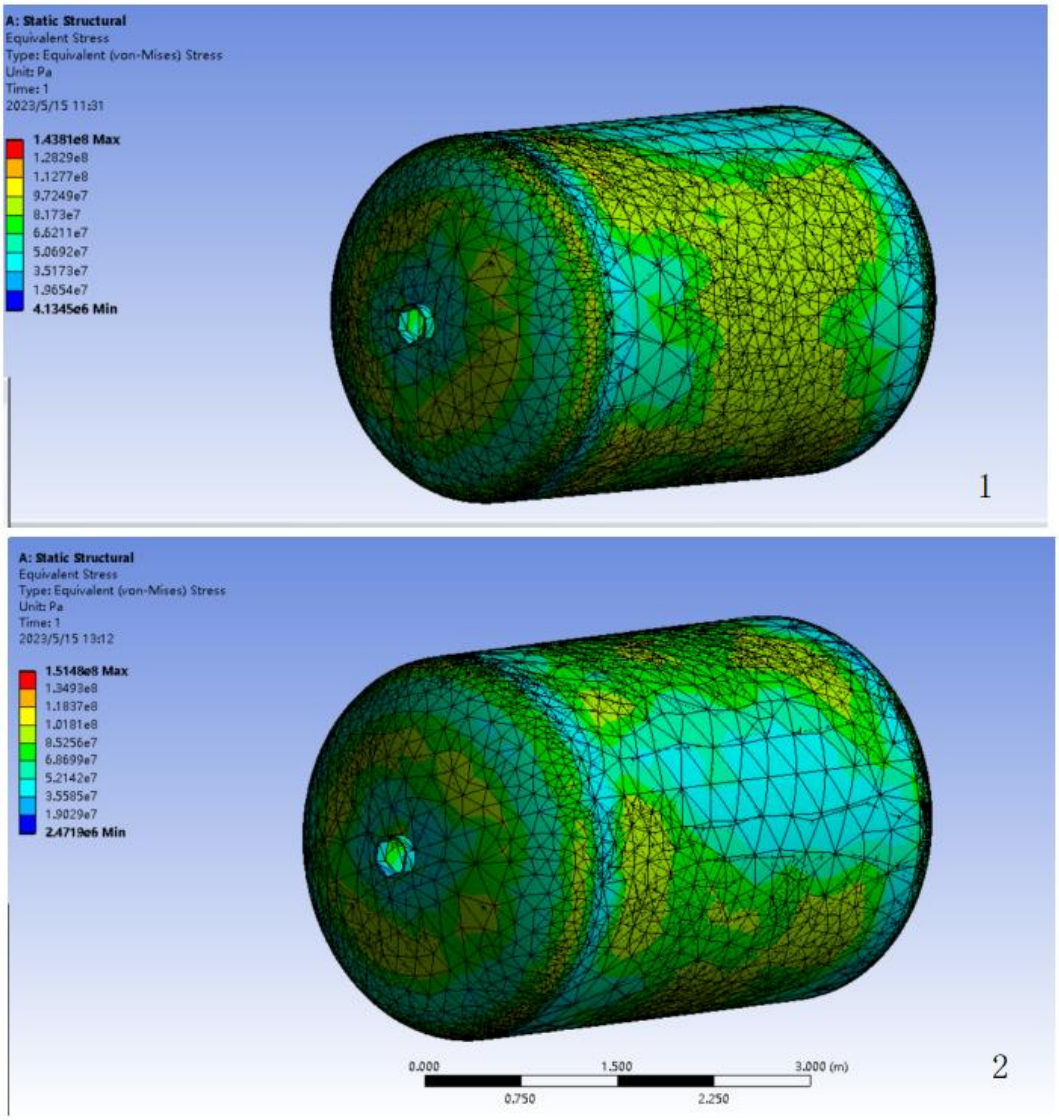

1. large deflection on; 2.large deflection off.

Figure 3.19 - The equivalent stress of the liquid hydrogen inner cylinder

As shown in the figure 3.20, a significant plastic strain occurred in the two end portions of the barrel, with a gradual minimum from the sides toward the middle. It can be inferred that the two end portions of the barrel are most likely to fail during the pressurization process.

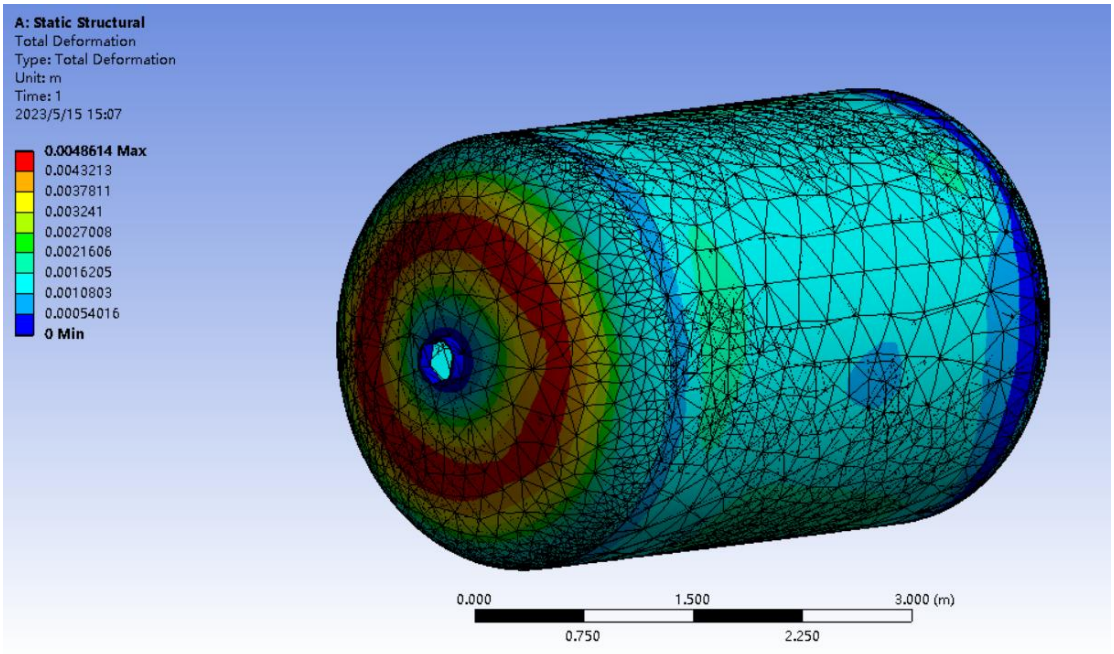

Figure 3.20 - The equivalent stress of the liquid hydrogen inner cylinder

When the input pressure increase 1.7MPa, the maxium equivalent stress reaches 520MPa, which is the yield pressure of material.

1.7MPa < 2.08MPa. The predicted burst pressure of the elastic-plastic analysis considering plastic deformation is less than the theoretical calculated value.

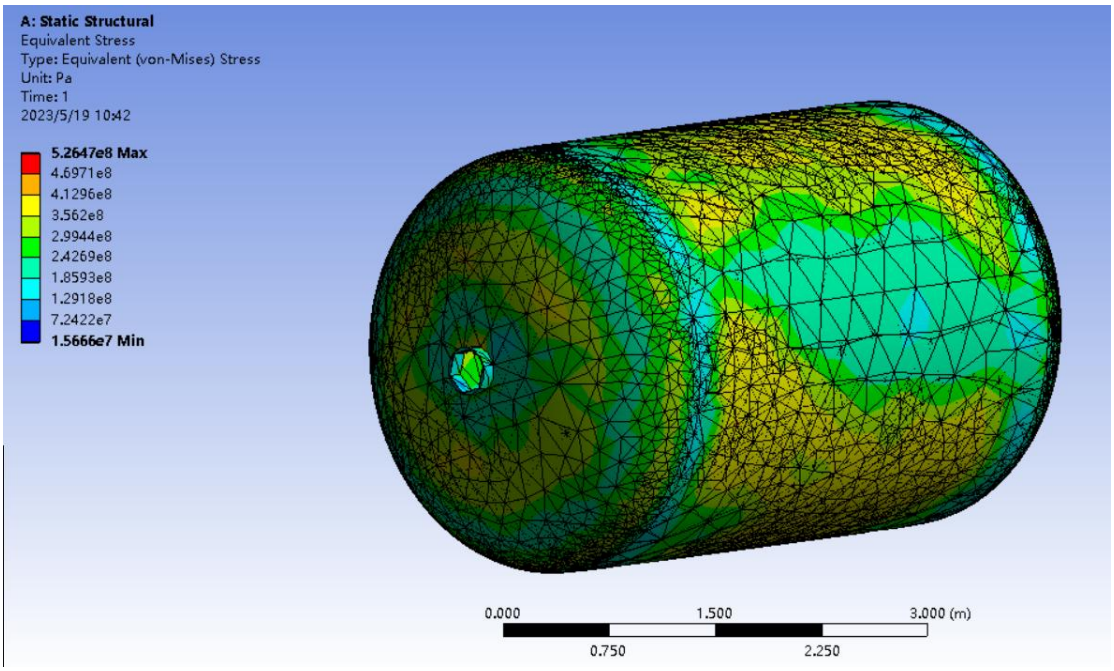

Figure 3.21 - The equivalent stress of the cylinder under P=1.7MPa

Besides, different fixing methods may lead to different stress results. This needs to be explored further.

4.3.6 Theoretical Buckling Analysis of outer container:

In addition to the load transmitted from the inner support structure, the outer cylinder surface is only subjected to atmospheric pressure. The main failure modes of the container under external pressure are strength failure and buckling, of which buckling is the main failure mode. Therefore, it is necessary to perform buckling analysis on the outer container.

The critical length L_{cr} is used as the boundary to distinguish between long and short cylinders and rigid cylinders. The calculation of it is:

$$L_{cr} = 1.17 D_0 \sqrt{\frac{D_0}{t_1}}$$

Where, D_0 - the diamater of the outer container, mm;

t_1 - the thickness of outer diameter to inner diameter, mm.

$$L_{cr} = 1.17 \times 3100 \times \sqrt{\frac{3100}{9}} = 67314.3mm$$

Length of outer container is 5.3m, which is less than 67.3m. Thus it is belongs to short cylinder. In this case, the buckling wave number n is calculated by:

$$n = (7.06 / ((L / D)^2 (t / D)))^{1/4}$$

Where, D - the mid diamater of the outer container, mm;

L - the length of outer container, shown in figure 3.21, mm.

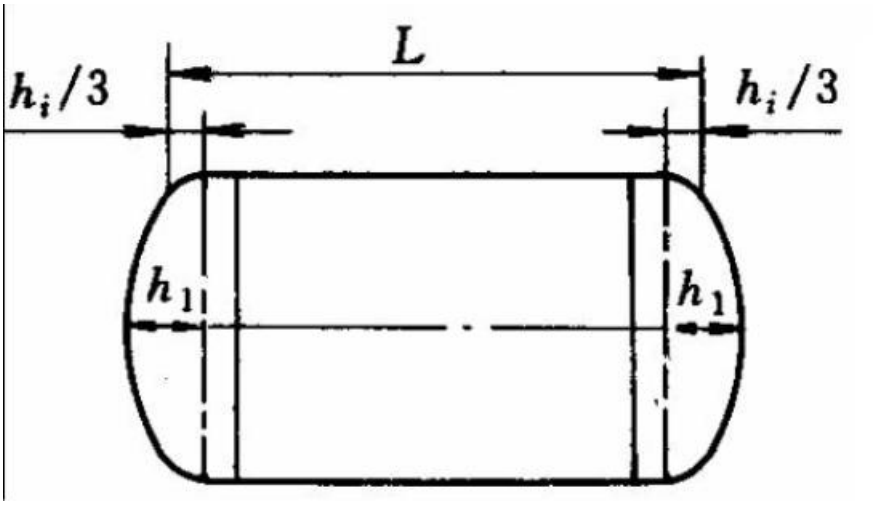

Figure 3.22 - The scheme of the length of outer container

$$L = 5300 - 700/3 \times 2 \times 2 = 4367\ mm$$

$$n = (7.06/((4367/3091)^2(9/3091)))^{1/4} = 5.9$$

Here we take n = 6. And some examples of different buckling wave numbers are shown in figure 3.22.

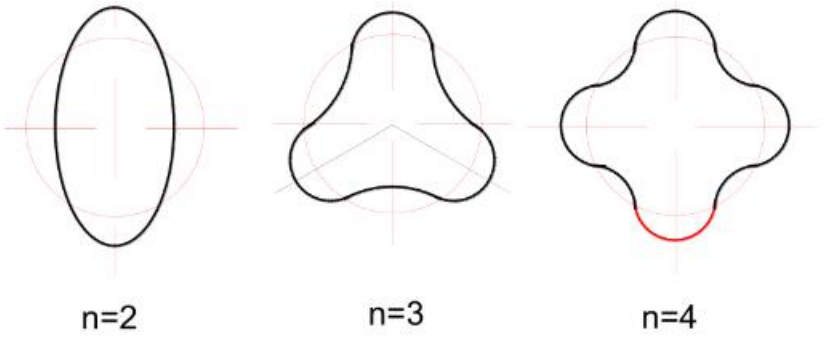

Figure 3.23 - The shape of an externally pressed cylinder after circumferential buckling

For short containers subjected to uniform external pressure, ASME VIII-1 specification is used and the critical pressure P_{cr} formula can be calculated:

$$P_{cr} = \frac{2.59E(\delta_e/D_0)^{2.5}}{L/D_0}$$

Where, D_0 - the outer diamater of the outer container, mm;

E - the elasticity modulus of the material, MPa;

δ_e - the thickness of the container, mm.

$$P_{cr} = \frac{2.59 \times 207000 \times (9/3100)^{2.5}}{4367/3100} = 0.17 MPa$$

Therefore, the structure will not be damaged by buckling under normal pressure.

.

3.4 Conclusions

In this part, we review and prospect the sustainable aircraft. Different energy sources and their applications are discussed, especially the liquid hydrogen. It has the characteristics of high efficiency, stability and non-pollution. We also finish the calculation and ansysis on Ultimate Bearing Capacity of Cryogenic Liquid Hydrogen Cylinder in hydrogen aircraft by using the numerical calculation method through the finite element software workbench.

However, considering its size and weight, liquid hydrogen storage tanks made of composite materials will be lighter and less costly in the long run.

Apart from the application of new energy sources, there are many other ways to reduce aircraft carbon emissions. For example, reducing the weight of the aircraft, using new composite materials, environmental-friendly materials, optimizing the structure, improving efficiency during taxi, takeoff and landing, optimizing flight trajectories, etc. Throughout history, scientific breakthroughs often require innovation and a spirit of adventure. At the same time the power of science and technology is infinite, we believe that the future world must be a world where new technology, new energy and new materials are widely used.

CONCLUSIONS

The master degree thesis consists of the following main parts: the first part concentrates on the aircraft preliminary design, the calculation of geometrical and aerodynamic parameters and other basic information about the aircraft. This type of aircraft has excellent performances which is in line with the requirement of new airline.

The second part of master thesis is devoted to calculate the cost of aircraft and its operation. And we got its ticket price and profit of the aircraft per ton per kilometer.

In the third part of the thesis, we reviewed the Development of sustainable aircraft and liquid hydrogen storage. Besides, The special work focuses on the engineering application, and the preliminary exploration on the liquid hydrogen storage scheme, material selection, structural modeling and numerical calculation of liquid hydrogen cylinder has been carried out. We analyse the limit load carrying capacity. UG is used to model the structural elements and Workbench is used to simulate the stress-strain state of the cylinder under the loads. From the results of many simulations by Ansys, this type of design have great properties to endure the load.

However, there are some works for me to imrprove and finish in the future. First of all, when predicting the ultimate load carrying capacity of the gas cylinder liner, the influence of various pipes is not considered. So further research needs to consider modeling the structural receiver to supplement it and make it more perfect.

Secondly, we only theoretically calculate the wave number and critical buckling load of the outer container without establishing a three-dimensional numerical model to simulate and analyze its actual situation in Workbench.

At last, fatigue analysis is also needed for the container. When transporting liquid hydrogen onboard, the cylinder is subjected to cyclic stresses due to temperature changes and inertia forces inflight. It is necessary to analyze its fixtures accordingly.

REFERENCE

[1] Chen Nongtian, Ning Weifeng, Chen Jun, et al. A review of airworthiness safety issues of new energy aircraft. Journal of Civil Aviation Flight University of China. Volume 33, September 2022.

[2] Abu Salem, K.; Palaia, G.; Cipolla, V.; Binante, V.; Zanetti, D.; Chiarelli, M. Tools and methodologies for box-wing aircraft conceptual aerodynamic design and aeromechanic analysis. Mech. Ind. 2021, 22, 39.

[3] Total CO2 Emissions Globally. Available from: https://www.carbonmonitor.org.cn/

[4] Chapman, A.; Fujii, H. The Potential Role of Flying Vehicles in Progressing the Energy Transition. Energies 2022, 15, 7406.

[5] T. Phillips. 10 Solar-Powered Airplanes That Changed the World. Available from: https://aerocad2.com/10-approaches-used-for-solar-powered-airplanes

[6] NASA. Available from: https://www.nasa.gov/specials/X57/index.html

[7] Liu C, Doulgeris G, Laskaridis P, et al. Thermal cycle analysis of turboelectric distributed propulsion system with boundary layer ingestion. Aerosp Sci Technol 2013, 27(1):163–70.

[8] NASA. Available from: https://sacd.larc.nasa.gov/asab/asab-projects-2/starc-abl

[9] Guy Norris. Rolls-Royce Unveils All-Electric ACCEL Aircraft. Available from: https://aviationweek.com/business-aviation/rolls-royce-unveils-all-electric-accel-aircraft

[10] Ren Zhilu. Will hydrogen aircraft become a new blue ocean for the aviation industry. JETLINER, 2022, 9: 45-48.

[11] Airbus. Available from: https://www.airbus.com/en/innovation/zero-emission-journey/hydrogen/zeroe

[12] The British presented the concepts of three hydrogen aircraft. Available from: https://vpk.name/en/587269_the-british-presented-the-concepts-of-three-hydrogen-aircraft.html

[13] Xiao Wenzheng, Ma Zhimin, Wang Zhi. Research and prospect of new aviation biofuel. Chemical Enterprise Management, 2018.

[14] Ji Yuhan, Sun Xiasheng, Yu Xiao, et al. Development prospect of n ew energy aviation under carbon peaking and carbon neutrality goals [J]. Aeronautical Science & Technology, 2022, 33(12):1-11.

[15] Ren Zhilu. Will hydrogen aircraft become a new blue ocean for the aviation industry. JETLINER, 2022, 9: 45-48.

[16] SCHLAPBACH L, ZüTTEL A. Hydrogen-storage materials for mo bile applications[J]. Nature, 2001, 414(6861): 353–358

[17] ZÜTTEL A. Materials for hydrogen storage[J]. Materials Today, 20 03, 6(9):24–33.

[18] SAZELEE N A, ISMAIL M. Recent advances in catalyst-enhanced LiAlH4 for solid-state hydrogen storage: a review[J]. International Jo urnal of Hydrogen Energy, 2021, 46(13): 9123–9141.

[19] Yang J, Sudik A, Wolverton C, et al. High capacity hydrogen storag e materials: Attributes for automotive applications and techniques for materials discovery. Chem Soc Rev, 2010, 39: 656−675.

[20] Status and development of hydrogen preparation, storage and trans portation (in Chinese). Chin Sci Bull, 2022, 67: 425-436. DOI: 10.136 0/TB-2021-0715.

[21] XU Shuo YU Biying. Current Development and Prospect of Hydro gen Energy Technology in China. Journal of Beijing lnstitute of Techn ology(Social Science Edition), 2021, 23(6). DOI: 10.15918/j.jbitss100 9-3370.2021.3061.

[22] CHEN Xiaolu, LIU Xiaomin,WANG Juan,et al. Technology and sta ndarlization of liquid hydrogen storage and transportation[J]. Chemic al Industry and Engineering Progress, 2021, 40(9): 4806-4814.

[23] Shen Jun. Limit Load Analysis Application in Pressure Vessel Anal ytical Design[J]. Petro-chemical equipment, 2011, 40(4):35-38.

[24] Bai Haiyong, Fang Yongli. ANSYS Limit Load Analysis Method in Pressure Vessel Design[J]. Pressure Vessel Technology, 2014,31(6):4 7-50.

[25] Airbus. Available from: https://www.airbus.com/en/newsroom/new s/2021-12-how-to-store-liquid-hydrogen-for-zero-emission-flight.

[26] QIU Y N, YANG H, TONG L G, et al. Research progress of cryoge nic materials for storage and transportation of liquid hydrogen[J]. Met

als, 2021, 11(7): 1101.

[27] KIM J H, CHOI S W, PARK D H, et al. Charpy impact properties of stainless steel weldment in liquefied natural gas pipelines: Effect of low temperatures[J]. Materials & Design, 2015, 65: 914-922.

[28] Zhang Xiaobing. Research on Ultimate Bearing Capacity of Cryogenic Liquid Hydrogen Cylinder[D]. Taiyuan: Taiyuan University of Technology, 2020.

[29] Chen Ding, Chen Zhenhua. Mechanical Properties of Pure Aluminum Alloys at Cryogenic Temperatures. Aerospace Materials & Technology, 2000, 4:1-7.

[30] Fesmire JE, Swanger AM. Advanced cryogenic insulation systems. International Congress of Refrigeration. Montreal, Quebec, Canada: Intl Institute of Refrigeration; Aug 2019.